2016

Delineating ÎNp63Î±'s function in epithelial cells

Suraj Sakaram
Wright State University

Delineating ΔNp63α's function in epithelial cells

A thesis submitted in partial fulfillment
of the requirements for the degree
of Master of Science

By

SURAJ SAKARAM
B.S., The Ohio State University, 2014

2016
Wright State University

WRIGHT STATE UNIVERSITY

GRADUATE SCHOOL

October 10, 2016

I HEREBY RECOMMEND THAT THE THESIS PREPARED UNDER MY SUPERVISION BY Suraj Sakaram ENTITLED Delineating ΔNp63α's function in epithelial cells BE ACCEPTED IN PARTIAL FULFILLMENT OF THE REQUIREMENTS FOR THE DEGREE OF Master of Science.

Madhavi Kadakia, Ph.D.
Thesis Director

Madhavi Kadakia, Ph.D.
Department Chair

Committee on Final Examination

Madhavi Kadakia, Ph.D.

Michael Raymer, Ph.D.

Weiwen Long, Ph.D.

Robert E. W. Fyffe, Ph.D.
Vice President for Research and
Dean of the Graduate School

ABSTRACT

Sakaram, Suraj. M.S. Department of Biochemistry and Molecular Biology, Wright State University, 2016. **Delineating ΔNp63α's function in epithelial cells.**

ΔNp63α, the most physiologically relevant isoform of p63, a p53 family member protein, maintains the proliferative capacity of the basal layer of epithelial tissues and is highly expressed in non-melanoma skin cancer. It has been implicated in a variety of different cancers, including breast, lung, and prostate cancers, however the complex role it plays in disease remains poorly understood. Elucidating ΔNp63α's regulatory network may provide insight into its role in epithelial tissues and in cancer progression. The objective of this thesis is to investigate ΔNp63α's upstream regulation in the context of non-melanoma skin cancer as well as expand on ΔNp63α's downstream function through its modulation of target microRNAs (miRNAs).

Non-melanoma skin cancer is primarily a result of excessive exposure to ultraviolet (UV) radiation. ΔNp63α appears to be regulated by post-translational modifications such as phosphorylation, which can lead to its degradation in a ubiquitin-mediated, proteasome-dependent manner. cJun N-terminal kinase (JNK), a stress activated protein kinase (SAPK), is potently activated by UV stress and has been shown to phosphorylate p53 and p73. I hypothesized that UV-induced JNK activation can similarly regulate ΔNp63α via phosphorylation. Anisomycin and UV induced JNK activation were shown to produce an electrophoretic mobility shift in ΔNp63α, suggesting it was phosphorylated. Co-expression of JNK and ΔNp63α also exhibited an enhanced electrophoretic mobility shift in ΔNp63α following UV and anisomycin treatment. Phosphorylation was confirmed using an *in vitro* kinase assay with recombinant JNK and p63 proteins. Mass spectrometry analysis of immunoprecipitated ΔNp63α protein from UV treated

H1299 cells transfected with ΔNp63α and *in vitro* kinase assay samples identified several phosphorylated residues, some of which are highly conserved in p73. Mutation of these potential JNK targeted residues alone did not prevent an electrophoretic mobility shift, however, a combination of mutated residues resulted in a stabilization of ΔNp63α levels. These results suggest that JNK plays a role in the phosphorylation of ΔNp63α, implicating it as a potential mediator of ΔNp63α degradation and apoptosis.

ΔNp63α has been shown to regulate a number of miRNAs that affect a wide range of biological processes. Advances in high-throughput sequencing technologies have made it possible to profile differentially expressed miRNAs to gain insight into the role they play in the pathogenesis of cancer. Interestingly, although next-generation sequencing (NGS) platforms have become popular for studying miRNA expression profiles through small RNA-Seq, a consensus on the data processing methodology has not yet been reached. In this dissertation, I sought to both optimize and validate a pipeline for analyzing small RNA-Seq data and, with the resulting dataset, gain insight into the regulation of miRNA expression by ΔNp63α. A test NGS dataset was generated by sequencing small RNA from non-silencing control (NSC) and p63-silenced (sip63) HaCaTs cells using the Ion Proton™ System. I optimized data collection and analysis parameters using this dataset and established a functional pipeline workflow involving alignment to the miRBase reference database, normalization using the Trimmed Mean of M-values (TMM) normalization method, and differential expression using a lognormal with shrinkage response distribution model. This pipeline configuration resulted in a shortlist of differentially expressed miRNAs which was enriched for known p63-regulated miRNAs, thus empirically confirming pipeline function. Finally, I validated the differential expression of several novel p63-regulated

miRNA including miRs-103a-3p, 149-5p, 18a-5p, 19b-1-5p, 590-5p, 598-3p, 7-5p, 708-5p, 744-5p, and 93-5p.

In Summary, this study provides insight into JNK's potential regulation of ΔNp63α via phosphorylation and downstream proteasomal degradation. As well, optimization of a small RNA-Seq pipeline facilitated identification of novel ΔNp63α-regulated miRNAs and expanded our understanding of the role played by ΔNp63α in cancer progression.

TABLE OF CONTENTS

LIST OF FIGURES

Figure **Page**

LIST OF TABLES

ACKNOWLEDGMENTS

I would like to express my sincerest gratitude to my Masters advisor, Dr. Madhavi Kadakia, for being an incredible mentor who has provided me not only a second chance, but also an opportunity to grow and develop as a scientist and an individual. I am truly thankful for her patience and guidance through all the ups and downs I have had in the laboratory and outside of it. It suffices to say that I would not be the person I am today without the immense help, teachings, and wisdom I have received under her tutelage. She resembles the person I strive to be and reminds me to keep my nose to the grindstone and pay it forward. Thank you for all your help and guidance, Dr. Kadakia! I would also like to sincerely thank my committee members, Dr. Michael Raymer and Dr. Weiwen Long, for their expertise on my research projects and guidance in completing my thesis.

A special thanks to all the past and present Kadakia lab members who I have had the pleasure to work with. I would like to recognize Dr. Natasha Hill, Dr. Michael Craig, Dr. Jin Zhang, Andrew Stacy, Reilly Clark, Amal Albati, Amjad Aljagthmi, and Zach Smith. I thank you for all the support and guidance you have given me. You all made it a joy to come into lab every day and amidst our conversations, I have learned a great many life lessons and shared a great many laughs, both of which I cherish dearly. I would also like to thank the Biochemistry and Molecular Biology department for providing such a warm, welcoming atmosphere in addition to technical expertise and encouragement.

I am also very thankful for all my friends whose love and support have been with me throughout my time as a graduate student. Thank you specifically to one of my best friends, Muskan Gupta. I am glad that our respective academic journeys happened to put us at the same institution. I am truly grateful for her love and support – she is my go-to for most things in life and

has been there for me when I needed it most. Last but certainly not least, I would like to sincerely thank my family for all their love and support – my brother especially for always being resourceful and helpful with anything and everything, my father for always encouraging me to strive for more, and my kind-hearted mother for her continued belief in me. They mean the world to me and I am nothing without them. A million thanks for everything!

DEDICATIONS

I would like to dedicate this thesis in its entirety to my hero. I hope when you look back on this, the lessons you learned are not lost. Let this work serve as a reminder that hard work, passion, and focus are ultimately what will help you make a dent in the universe.

I. INTRODUCTION

A. ΔNp63α and the skin

p63 is a p53 family member protein that is primarily expressed in the basal layer of the epidermis and other epithelial tissues. It plays an integral role in developing these tissues and maintaining their proliferative capacity. The p63 gene contains an N-terminal transactivation domain (TA), a central DNA binding domain (DBD), and a C-terminal oligomerization domain (OD), sequences that share high homology to p53 and p73 (Yang, Kaghad et al. 1998). Due to alternative promoter usage and 3'-terminal splicing, p63 can be transcribed as multiple isoforms. Transcription initiated at the P1 promoter produces the full-length TA domain isoforms whereas transcription initiated at the internal P2 promoter produces the truncated TA domain (ΔN) isoforms. Differential 3' splicing yields the full-length (α), or truncated (β or γ) isoforms (**Fig. 1**) (Yang, Kaghad et al. 1998, Courtois, Caron de Fromentel et al. 2004). TAp63 isoforms function similarly to p53 by acting as tumor suppressors, while ΔNp63 isoforms antagonize p53 and TAp63-mediated transactivation of target genes. ΔNp63 can also transactivate select target genes (Senoo, Matsumura et al. 2002, Osada, Park et al. 2005, Kommagani, Caserta et al. 2006, Ortt, Raveh et al. 2008, Marinari, Ballaro et al. 2009).

p63 is essential for proper development of limbs and stratified epithelium as was demonstrated in p63 null mice which lacked skin and limbs, and died shortly after birth due to dehydration (Mills, Zheng et al. 1999, Yang, Schweitzer et al. 1999). The ΔNp63α isoform is the most abundantly expressed and physiologically relevant isoform. It is expressed in the basal layer of the epidermis where it functions to maintain epithelial stemness (Pellegrini, Dellambra et al. 2001, Koster and Roop 2004). As keratinocytes differentiate into the upper levels of the epidermis,

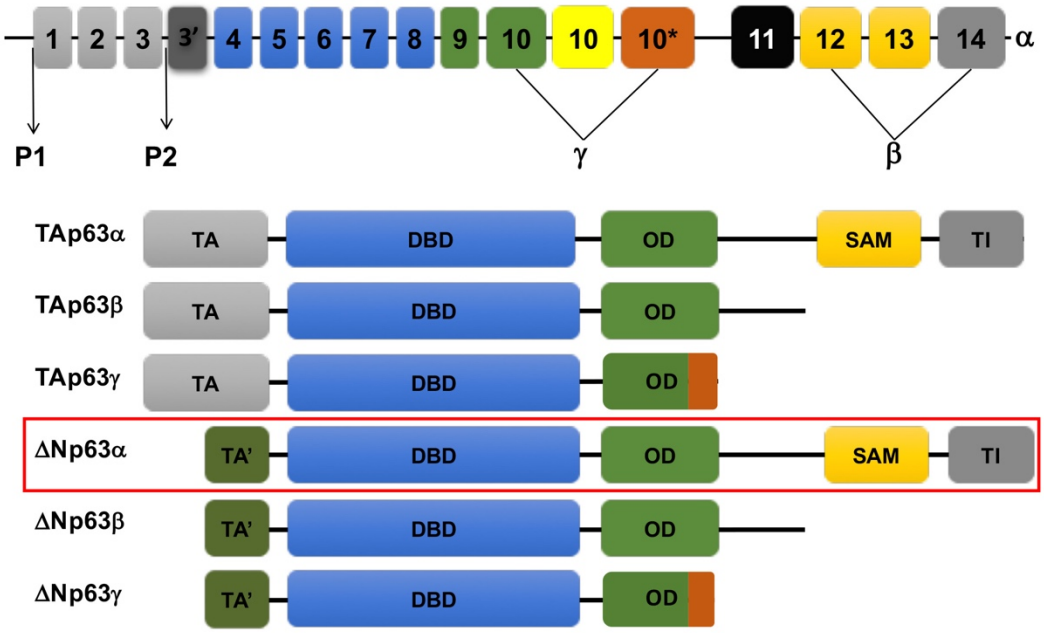

Figure 1: p63 isoforms. Schematic of the p63 gene comprising of the two promoter sites, 3' splicing segments, and the resulting six main p63 isoforms. The domains are as follows: transactivation domain (TA), DNA-binding domain (DBD), oligomerization domain (OD), sterile alpha motif (SAM), and transactivation inhibitory domain (TI).

cells lose their proliferative capacity as a result of a decrease in ΔNp63α expression levels (Koster and Roop 2004) (**Fig. 2**).

B. ΔNp63α and Non-melanoma skin cancer

There are approximately 5 million new cases of non-melanoma skin cancer (NMSC) each year (Rogers, Weinstock et al. 2015). The two main types are basal cell carcinoma (BCC) and squamous cell carcinoma (SCC). BCC occurs in the basal layer of the epidermis and rarely metastasizes, whereas SCC occurs in the squamous cell keratinocytes of the outer layers of the epidermis with the potential to metastasize (Safai and Good 1977). One of the main hallmarks of these cancers is an increased expression of the proto-oncogene, ΔNp63α (Reis-Filho, Torio et al. 2002, Lo Muzio, Santarelli et al. 2005, Bircan, Candir et al. 2006). Numerous studies have implicated ΔNp63α in promoting tumorigenesis via enhanced AKT activation through inhibiting transcription of PTEN and positively regulating epidermal growth factor receptor leading to an increase in pancreatic cancer cell proliferation (Danilov, Neupane et al. 2011, Leonard, Kommagani et al. 2011). Interestingly, loss of ΔNp63α has shown to promote cancer progression in prostate, bladder, and breast cancer as well as increased motility and cell invasion indicating that p63 has a complex role in mediating cancer progression (Di Como, Urist et al. 2002, Medina-Franco, Vasconez et al. 2002, Senoo, Matsumura et al. 2002, Urist, Di Como et al. 2002, Barbieri, Tang et al. 2006, Carroll, Carroll et al. 2006, Kommagani, Leonard et al. 2009).

The primary cause of NMSC is thought to be excessive exposure to ultraviolet (UV) radiation, a form of genotoxic stress that can cause DNA lesions, such as cyclobutane pyrimidine dimers and 6,4-photoproducts (Boukamp 2005). UV-induced lesions result in programmed cell death mediated by c-Jun N-terminal kinase (JNK) and p38 pathways (Zhang and Bowden 2012).

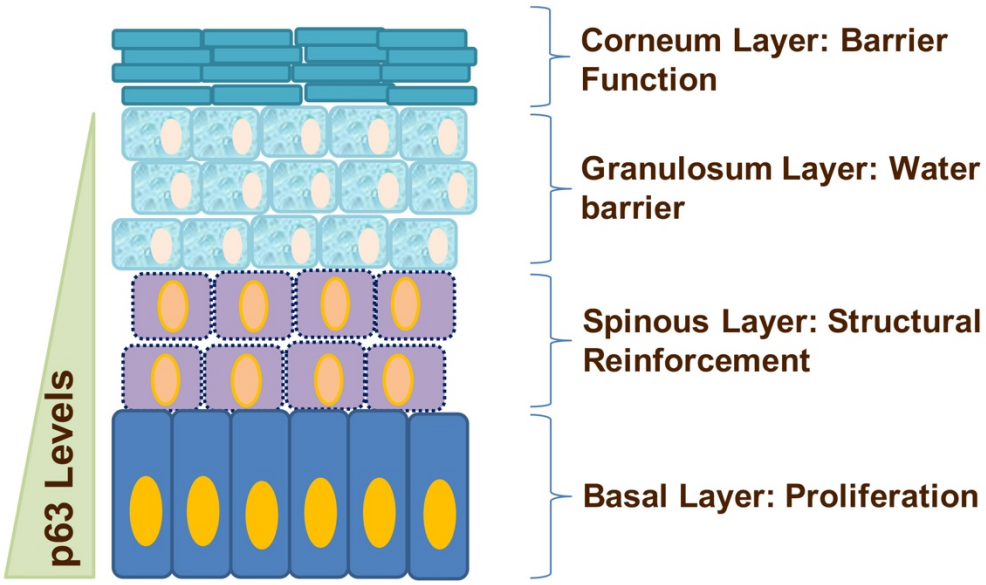

Figure 2: Diagram of epidermal stratification. The epidermis consists of four layers starting with the basal layer, where ΔNp63α is highly expressed, to the terminally differentiated corneum layer. ΔNp63α levels decrease as the keratinocytes differentiate into the upper layers of the epidermis.

Furthermore, for apoptosis to occur in keratinocytes, UV-mediated down-regulation of ΔNp63α is required (Liefer, Koster et al. 2000). However, this is not the case as ΔNp63α is overexpressed in NMSC, suggesting that normal apoptotic factors are being inhibited.

C. ΔNp63α and phosphorylation

p63 is phosphorylated following UV treatment, as evidenced by an electrophoretic mobility shift in ΔNp63α and ablated by treatment with alkaline phosphatase (Westfall, Joyner et al. 2005). While phosphorylation of TAp63 proteins result in their accumulation, studies have demonstrated that phosphorylated ΔNp63α is ubiquitinated and degraded in a proteasome dependent mechanism, leading to programmed cell death, such as phosphorylation of p63 by Dlx3 during development, HIPK2 in response to genotoxic drugs, or ALK5 in response to UV (Katoh, Aisaki et al. 2000, Okada, Osada et al. 2002, Papoutsaki, Moretti et al. 2005, Westfall, Joyner et al. 2005, Di Costanzo, Festa et al. 2009, Lazzari, Prodosmo et al. 2011). In contrast, c-Abl tyrosine kinase can phosphorylate tyrosine residues on ΔNp63α inducing its association with Yes-Associated Protein (YAP), leading to increased ΔNp63α stability, cell proliferation, and protection from cisplatin-induced cell death, thus suggesting that the site of phosphorylation on ΔNp63α may dictate its resulting stability and function (Yuan, Luong et al. 2010).

Previous studies have shown that cellular stress resulted in the activation of the p38 pathway, leading to the phosphorylation of ΔNp63α. UV-induced lesions in normal keratinocytes induce apoptosis mediated by the p38 pathway (Raingeaud, Gupta et al. 1995). Our laboratory has also shown that low doses of Vitamin D_3 led to an increase in ΔNp63α protein levels and keratinocyte proliferation via activation of p38 and Akt (Hill, Zhang et al. 2015). Furthermore, inhibition of p38 has been shown to repress the electrophoretic mobility shift observed in ΔNp63α

following UV irradiation, while cells overexpressing constitutively active upstream kinases of p38 show an enhanced mobility shift (Papoutsaki, Moretti et al. 2005).

UV-treated keratinocytes also show an increase in activated JNK levels, leading to apoptosis (Hibi, Lin et al. 1993, Derijard, Hibi et al. 1994). Although phosphorylation of ΔNp63α by p38 has been documented, a related stress-activated kinase, JNK, has not been eliminated as a candidate kinase of ΔNp63α (Papoutsaki, Moretti et al. 2005).

D. JNK

JNK, a stress activated protein kinase (SAPK), is encoded by three different genes (JNK1-3) that may be differentially spliced to produce at least 10 different isoforms (Zhang and Selim 2012). JNK signaling is implicated in a wide range of cellular processes such as cell survival, proliferation, differentiation, and apoptosis (Hu, Qiu et al. 1997, Buschmann, Potapova et al. 2001, Wu 2004, Bode and Dong 2007, Zhang and Selim 2012). JNK1 acts as a tumor suppressor while JNK2 is a potent tumor promoter found to be overexpressed in conjunction with its downstream substrate, c-Jun, in squamous cell carcinoma, basal cell carcinoma, and melanoma (Hochedlinger, Wagner et al. 2002, Sabapathy, Hochedlinger et al. 2004, Bode and Dong 2007, Zhang and Bowden 2012). Active JNK is known to directly phosphorylate p53 in response to cellular stress and DNA damage, stabilizing protein levels while decreasing ubiquitination and increasing transcriptional activity (Hu, Qiu et al. 1997, Fuchs, Adler et al. 1998, Buschmann, Potapova et al. 2001, Wu 2004, Park, Kim et al. 2016). Phosphorylation of p53 at serine-34 and threonine-81 has shown to upregulate p53 transcriptional activity correlating with increased cell cycle arrest and induction of apoptosis, respectively (Hu, Qiu et al. 1997, Buschmann, Potapova et al. 2001). Studies have shown JNK to be required for p73-mediated apoptosis. JNK phosphorylates p73 on

at least seven different residues located in both the N-terminus and C-terminus where phospho-deficient mutations of these sites prevent p73-mediated apoptosis. These sites are highly conserved in ΔNp63α (Jones, Dickman et al. 2007). Although ΔNp63α shares conserved residues with other known JNK targets in the p53-family of proteins, JNK-mediated phosphorylation of ΔNp63α has not been reported.

E. Downstream targets of ΔNp63α: miRNAs

microRNAs (miRNAs) are small non-coding RNAs (approximately 18-22 nucleotides in length) that post-transcriptionally regulate gene expression. They are able to bind to 3' UTR regions of target mRNA and translationally repress or degrade them (Lewis, Burge et al. 2005). They can also interact with the protein coding regions of mRNA (Helwak, Kudla et al. 2013). miRNAs are derived from intragenic regions of the genome as well as introns of pre-mRNAs and undergo two processing steps involving ribonucleases to produce mature miRNAs. Initially, a long primary transcript (pri-miR) is transcribed by RNA polymerase II and in some cases RNA polymerase III, resulting in a stem-loop structure with a 5' cap and 3' poly-A tail (Bartel 2004, Lee, Kim et al. 2004, Borchert, Lanier et al. 2006). pri-miRNAs are modified by the Drosha complex (an RNase III enzyme in complex with DGCR8 and several auxiliary factors) to produce hairpin structured precursor miRNAs (pre-miRNAs), which are approximately 70 nucleotides in length. pre-miRNAs are transported out of the nucleus via Exportin-5 (XPO5) and Ran-GTP (Zeng and Cullen 2004). In the cytoplasm, pre-miRNAs are processed by Dicer, another RNase III enzyme, to form mature duplex miRNAs. One of the strands of the miRNA duplex is loaded onto the RNA-induced silencing complex (RISC), which contains Argonaute (Ago), and serves as a guide to direct RISC to target mRNAs and either degrade, destabilize, or translationally inhibit

their expression (Bartel 2009, Jansson and Lund 2012). A single miRNA may target hundreds of genes and a single mRNA may be targeted by hundreds of miRNAs, thus the dysregulation of several miRNAs can have strong biological effects on entire gene networks. miRNAs may regulate key components of various cellular processes such as proliferation, differentiation, apoptosis, motility & invasion, morphogenesis, and survival as it is estimated that they may regulate over a third of all mammalian genes (Lewis, Burge et al. 2005, Irani 2016). miRNA have been used as novel biomarkers for cancer diagnosis. Understanding miRNA expression profiles for various cancers has helped to better classify poorly differentiated tumors (Lu, Getz et al. 2005, Wojcicka, Kolanowska et al. 2016).

F. ΔNp63α regulation of miRNAs

ΔNp63α has been shown to modulate the expression of miRNAs which can have profound effects on a number of cellular processes such as regulation of keratinocyte differentiation, cell migration, tumor growth, cell cycle arrest, apoptosis, and metabolism just to name a few (Ratovitski 2013, Lin, Li et al. 2015, Rodriguez Calleja, Jacques et al. 2016). Whereas ΔNp63α can transcriptionally activate a number of miRNAs, it also plays a role in the post-transcriptional processing of miRNAs specifically by acting on the Drosha complex and Dicer. It's been shown that ΔNp63α transcriptionally activates DGCR8 in the Drosha complex and could possibly interact with it through a PY-WW domain interaction (Chakravarti, Su et al. 2014). Furthermore, ΔNp63α regulates other transcription factors that regulate miRNAs. For example, Runt-related transcription factor 1, (RUNX1) which regulates miR-424, was identified as a target of ΔNp63α (Ortt, Raveh et al. 2008, Masse, Barbollat-Boutrand et al. 2012). It is clear that ΔNp63α regulates miRNAs directly and indirectly and the resulting regulatory network implicates it in a variety of cellular

processes. We set out to elucidate the global regulation of miRNAs by ΔNp63α by obtaining a ΔNp63α regulated miRNA expression profile via small RNA-Seq.

G. small-RNA Seq and data processing workflow

In recent years, improvements in next-generation sequencing (NGS) technology has made small RNA-Seq possible – a high throughput technology that queries small RNA species such as miRNAs with unprecedented sensitivity and dynamic range. Small RNA-Seq is increasingly being used for the comprehensive profiling of miRNAs for the purposes of classifying and categorizing diseases such as cancer and their prognoses (Lin, Lin et al. 2014, Alisoltani, Fallahi et al. 2015, Kou, Qiao et al. 2015). Despite the increasing popularity of small RNA-Seq, there is no consensus on an optimized data processing pipeline for miRNA sequencing data. The general processing for any sequencing experiment consists of mapping the sequenced reads to a reference genome, quantifying the abundance of each feature into raw read counts, and normalizing the raw read counts for subsequent downstream analyses, such as differential expression analysis (Conesa, Madrigal et al. 2016). However, the effect of available options at each stage of processing have not been fully explored for processing miRNA sequencing data despite the fact that parameters at each step of the processing can have a strong impact on the downstream analysis and classification of significantly differentially expressed (DE) miRNAs. Thus, I sought to develop an optimized pipeline workflow suitable for the identification of DE miRNAs.

In addition to optimizing a pipeline for small RNA-Seq, I sought to further elucidate ΔNp63α's function in epithelial tissues by identifying novel ΔNp63α-regulated miRNAs. Using the optimized pipeline, I selected several miRNAs that were significantly differentially expressed by small RNA-Seq and which had no known link to ΔNp63α and validated them using quantitative

real-time PCR, which is considered the gold standard for confirming next-generation sequencing experiments. Validation of several miRNAs in addition to having a significant DE list that was enriched for previously identified ΔNp63α-regulated miRNAs suggested that the pipeline was robust for the practical analysis of small RNA-Seq to identify differentially expressed miRNAs by a given transcription factor.

H. Rationale:

ΔNp63α is essential for the maintenance of epithelial tissue integrity, but its role in UV-induced damage and other forms of cellular stress remain poorly defined. As well, being a proto-oncogene, it plays a role in various cellular processes that influences the progression of numerous cancers, yet its regulatory network has not been fully investigated.

ΔNp63α activity and turnover appear to be regulated post-transcriptionally, and post-translational modifications may dictate the functional contribution of ΔNp63α in response to cellular stress. I showed herein that both endogenous and exogenous JNK induced an electrophoretic mobility shift in ΔNp63α in response to UV or Anisomycin treatment due to phosphorylation at multiple ΔNp63α residues. JNK-mediated phosphorylation occurred rapidly, within 30 minutes of the aforementioned cellular stress, and preceded ΔNp63α protein degradation, thus suggesting that phosphorylation of ΔNp63α by JNK may be an immediate early driver of ΔNp63α degradation and apoptotic progression.

Likewise, to further elucidate ΔNp63α's regulatory network within epithelial tissues, I assessed the global miRNA expression profile within keratinocytes as regulated by ΔNp63α via small RNA-Seq. I optimized critical data-mining parameters for assessing miRNA sequencing data and performed differential expression analysis to identify miRNAs that were significantly

differentially expressed. This methodology afforded critical insights into the predicted downstream targets of ΔNp63α and suggested that ΔNp63α may regulate a number of pathways that mediate cancer progression. Validation of several miRNAs with no previous connection to ΔNp63α may provide critical information concerning ΔNp63α's role in maintaining epidermal integrity as well as determining tumorigenic fate.

II. MATERIALS AND METHODS

A. Cell culture, reagents, and plasmids

HaCaT, a non-tumorigenic immortalized human keratinocyte cell line, was obtained from Dr. Nancy Bigley (Wright State University). H1299, a human non-small cell lung carcinoma cell line, which is null for p63 was used for overexpression studies. Both cell lines were maintained using DMEM Hyclone media supplemented with 8% fetal bovine serum and 100U/mL penicillin and streptomycin (referred to as complete media) at 37ºC in 5% CO_2. UVC treatments were carried out using the UV Stratalinker 1800. Anisomycin was prepared in DMSO as 1 mg/ml stock solution.

Expression plasmids encoding ΔNp63α were made as described previously (Kommagani, Leonard et al. 2009). Expression plasmids encoding HA tagged JNK1 and HA tagged JNK2 were a kind gift from Dr. Anja Jaeschke at University of Cincinnati. Expression plasmids encoding single site phospho-deficient mutants of ΔNp63α (S53A, S66A, S369A, T397A, and T444A) were constructed by Genscript services. Expression plasmid encoding a multi-site phospho-deficient mutant of ΔNp63α (S53, S66, S361, S369, T288, T397, and T444) was constructed by Genscript services.

B. Transient transfections

Cells were seeded at 3.5 x 10^5 into 6 well plates or 1.0 x 10^6 into 6 cm cell culture dishes prior to the day of transfection. At approximately 75% cell confluency, transient transfections were performed using Lipofectamine 2000 (ThermoFisher Scientific, Carlsbad, CA, USA) with desired plasmids (1:2 DNA to Lipofectamine 2000) in Opti-MEM solution as previously described (Leonard, 2011). After 5 to 6 hours of incubation at 37°C, media was replaced with fresh complete

media. For all studies, a total of 2 μg (6 well plate) or 3 μg (6 cm cell culture dish) of desired expression plasmids were used, adjusted for quantity using an empty vector plasmid.

C. Immunoblot analysis

At the time of harvest, cells were washed with cold PBS and whole cell extracts were made by lysing the cells in a buffer containing the phosphatase inhibitor buffer (50mM Tris-HCl pH 8.0, 120 mM NaCl, 5 mM EGTA, 1 mM EDTA, 5 mM NaPP, 10 mM NAF, 30 mM PMSF, 0.2 mM PMSF, 1 mM Benzamidine, 0.1% NP-40, 100 nM $NaVO_4$) supplemented with protease inhibitor cocktail (catalog #P8340, Sigma-Aldrich, St. Louis, MO). Protein concentration was quantitated using Bicinichoninic acid assay (BCA) according to the manufacturer's instructions (ThermoFisher Scientific, Fremont, CA, USA). Equivalent amounts of protein were separated on 7.5% or 10% SDS-PAGE and transferred to PVDF membrane at 350 mA for 1 hour. Proteins were detected using the following antibodies: Mouse monoclonal anti-phospho-JNK (T183/Y185, 1:2,000, Cell Signaling), rabbit polyclonal anti-JNK (#9652, 1:1,000, Cell Signaling), rabbit polyclonal anti-phospho-cJun (S63, 1:1,000, Cell Signaling), rabbit polyclonal anti-p63 (N2C1, 1:2,000, GeneTex), mouse monoclonal anti-pan-p63 (4A4, 1:10,000, Cell Signaling), and monoclonal anti-β-actin (AC15, 1:10,000, Santa Cruz) antibodies were used to detect phospho-JNK, JNK, phospho-c-Jun, ΔNp63α, and β-actin, respectively. Appropriate horseradish peroxidase antibodies (Promega, Madison, WI, USA) were used as secondary antibodies for chemiluminescent detection with the Western Lightning Plus-ECL Chemiluminescent Substrate kit (Perkin Elmer, Waltham, MA).

D. Immunoprecipitation and Mass spectrometry

H1299 cells were plated in 6 cm dishes transfected with myc-tagged ΔNp63α and exposed to UVC or Anisomycin treatment as described. Protein extracts were obtained by lysing cells with p40 lysis buffer (1% IGEPAL, 150mM NaCl, 1mM DTT, 25mM Tris pH 7.39, 1% Na_3VO_4, 2.5mM NaF, 0.5mM Sodium Pyrophosphate) supplemented with protease inhibitor cocktail (catalog #P8340, Sigma-Aldrich, St. Louis, MO). Samples were pre-cleared with Protein A agarose beads (Santa Cruz) and rotated overnight at 4ºC with mouse monoclonal anti-myc-tag (9B11, 1:1000, Cell Signaling) or mouse monoclonal anti-p63 (4A4, 1:1000, Abcam) antibody. Protein was immunoprecipated using Protein A agarose beads and samples were separated via SDS-PAGE in duplicate for immunoblot analysis and Coomassie blue staining. Protein bands identified by immunoblot were excised from the Coomassie gel and assessed for post-translational modifications by mass spectrometry.

E. *in vitro* Kinase Assay

Recombinant active JNK1 with N-terminal His-tag (1 µl of 50 ng/µl working stock) (#14-327, EMD Millipore), recombinant active JNK2 with N-terminal His-tag (1 µl of 50 ng/µl working stock) (#14-329, EMD Millipore), and recombinant ΔNp63α (1 µg) proteins were incubated in a 30 µl reaction consisting of 3 µl of 10X Reaction buffer (500 mM Tris/HCl (pH 7.5), 1mM EGTA, 5mM DTT, 200 mM $MgCl_2$, 75 mM 2-glycerophosphate) and 50 µM ^{32}P γ-labeled ATP (2.5 µCi/reaction) or non-labeled ATP (for purposes of mass spectrometry) at 30°C for 30 min (brought up to 30 µl in sterile distilled water). Similar reactions were performed using recombinant active c-Jun (1-79) activation domain fused to GST (#420108, Calbiochem) as a positive control. 7 µl of 5X sample buffer were added to samples after the reaction, boiled at 95°C for 5 min, and the

proteins were resolved via SDS-PAGE. Gels were stained using Coomassie blue to visualize protein bands. Then, the gels were de-stained, let dry, and phosphorylation was detected via autoradiography.

F. siRNA Knockdown

Knockdown of p63 in HaCaT cells was performed following transfection with either siRNA against p63 (sip63) or non-silencing control (NSC) using Lipofectamine RNAi-Max as per the manufacturer's instructions (ThermoFisher Scientific, Carlsbad, CA, USA). The siRNA against p63 used in this study was purchased from Qiagen (Valencia, CA, USA) as previously described (Kommagani, Leonard et al. 2009, Clarke, Newman et al. 2015).

G. qRT-PCR - silencing confirmation and small-RNAseq validation

Total RNA was extracted from HaCaT cells transfected with siRNA against p63 (sip63) and non-silencing control (NSC) using the mirVana™ Paris™ Isolation kit according to the manufacturer's protocol (ThermoFisher Scientific, Carlsbad, CA, USA). 1 μg of total RNA input was used for cDNA synthesis using a TaqMan reverse transcription kit (ThermoFisher Scientific, Carlsbad, CA, USA). TaqMan based quantitative real-time PCR analysis was performed as previously described (Kommagani, Leonard et al. 2009). Assays on Demand (AODs) for p63 (Hs00978340_ml), normalized to GAPDH (4325792) (ThermoFisher Scientific, Carlsbad, CA, USA), were used. For miRNA RT-PCR, cDNA was synthesized from 10 ng of total RNA. Quantitative real-time PCR analysis was performed using the QuantStudio 7 Flex Real-Time PCR System using TaqMan 2× master mix and miRNA-specific AODs for hsa-miR-103a-3p (00439), hsa-miR-149-5p (002255), hsa-miR-18a-5p (002422), hsa-miR590-5p (001984), hsa-miR-7-5p

(000268), hsa-miR-708-5p (002341), hsa-miR-744-5p (002324), hsa-miR-93-5p (001090) normalized to RNU48 (001006) (ThermoFisher Scientific, Carlsbad, CA, USA). qRT-PCR was done in triplicate for each specific miRNA of interest for each sample and performed using 3 biological replicates of NSC and sip63 transfected HaCaT cells.

H. small RNA-Seq library preparation

Total RNA was isolated from HaCaT cells using the mirVana™ Paris kit and enriched for small RNA through size selection ethanol washes. For each library, 4 ng of small RNA was ligated to adapters containing a unique barcode (Ion Xpress RNA-Seq Barcode 1-16 Kit, ThermoFisher Scientific, Carlsbad, CA, USA). Small RNA samples were reverse transcribed to cDNA using adapter specific primers (Ion Total RNA-Seq kit v2.0, ThermoFisher Scientific, Carlsbad, CA, USA). cDNA samples were size-selected and amplified followed up by a clean-up step using nucleic acid magnetic beads (ThermoFisher Scientific, Carlsbad, CA, USA). cDNA samples were barcoded using Platinum PCR SuperMix High Fidelity polymerase with IonXpress RNA 3' Barcode primer and unique 5' Ion Xpress RNA-Seq Barcode Primers (reduced to 0.5 μl each) (Cat #4471250, Ion Xpress RNA-Seq Barcode 1-16 Kit, ThermoFisher Scientific, Carlsbad, CA, USA). The yield and size distribution of the cDNA libraries were assessed using the Agilent 2100 Bioanalyzer using the High sensitivity DNA chip (DNA1000 chip, #5067-1504, Agilent Technologies, Santa Clara, CA, USA). Total cDNA within the 50-300bp range is considered to be obtained from small RNA. Of particular interest, the 94-114bp range is considered cDNA library from miRNA. 7.5 picomoles of each barcoded library were pooled and clonally amplified onto Ion SphereTM Particles (ISPs) per the manufacturer's protocol (Ion OneTouch™ 200 Template Kit v2 DL kit) and enriched using the Ion OneTouch 2 ES system (ThermoFisher Scientific, Carlsbad,

CA, USA). Enriched ISPs were sequenced on the Ion Proton Next Generation Sequencing system using Ion P1 chip and Ion Total RNA Seq Kit v2 (ThermoFisher Scientific, Carlsbad, CA, USA) with 500 sequencing flows.

I. small RNA-Seq data analysis

Alignment and Quantification: Sequenced reads were assigned to their respective samples based on corresponding IonXpress barcodes and output in FASTQ format with corresponding base quality scores using the Ion Torrent software. FASTQ files were uploaded into Partek Flow (Partek Inc., St. Louis, MO, USA) for processing. Reads were initially trimmed on both ends based on a minimum Phred quality score of 20 and a minimum read length greater than 15 nucleotides after trimming (The default minimum read length is 25 nucleotides). High quality trimmed reads were mapped using three reference genomes (whole genome, RefSeq Transcripts v2 (05-02-2016), and miRBase mature miRNAs version 21) of the latest human genome assembly, hg38, using the Bowtie aligner, an ultrafast, memory-efficient alignment algorithm that aligns short DNA sequence reads to large genomes with a seed mismatch limit of 1 and minimum seed length of 10. At the command line, the bowtie options would be entered as such: bowtie –n 1 –l 10 (Langmead, Trapnell et al. 2009). To obtain raw read counts, uniquely mapped reads were quantified to miRBase version 21 using an Expectation Maximization (EM) algorithm (Do and Batzoglou 2008). EM is a process that resolves ambiguous mappings (i.e., if a read can align equally well to multiple transcripts) to best estimate true expression read counts for a sample. It does so by starting with an initial estimate of transcript abundance (uniquely mapped reads) and calculates weighted means of ambiguous reads. The weighted means are used to re-compute the global transcript abundances which are then used to re-compute newly weighted means. This process is iterated

until it converges, at which point the reads assigned to a particular locus are counted resulting in the raw read counts (Do and Batzoglou 2008).

Normalization: Raw read counts were normalized to account for differences in library sizes and coverage. Several normalization methods were evaluated, including (1) Total Count (TC) (Dillies, Rau et al. 2013), (2) Reads Per Kilobase per Million (RPKM) (Mortazavi, Williams et al. 2008), (3) Transcripts Per Million (TPM) (Li, Shen et al. 2009, Li and Dewey 2011), and (4) Trimmed Mean of M values (TMM) (Robinson and Oshlack 2010). All normalization methods included an offset value of 1. (A miRNA with 0 counts would otherwise affect statistical calculations when performing differential expression analysis).

Differential Expression (DE) Analysis: The model design for DE analysis was selected based on our experimental design which compared the three p63 silenced biological replicates (sip63) to the three non-silenced control replicates (NSC). We tested two response distribution approaches: (1) The multimodel approach, which fit the normalized reads for each miRNA to the best model type (normal, negative binomial, lognormal, or lognormal with shrinkage) based on the model which had the lowest Akaike information criterion and (2) the lognormal with shrinkage (LNS) approach, similar to the "limma-trend" implemented in the limma package (Law, Chen et al. 2014). The shrinkage factor accounts for gene-specific dispersion, improving reproducibility in a low replicate study. A low expression threshold filter is applied to filter out the proportion of miRNAs that have 0 read counts as they are not of interest in the study and would otherwise affect the overall estimated trend of dispersion and shrinkage of error terms, resulting in an inaccurate model. As well, these miRNAs cannot be modeled well by a continuous distribution such as lognormal. Each approach generated statistical values such as p-value using the F statistic.

Principal Components Analysis (PCA): PCA is an exploratory data technique that reduces the dimensionality of a dataset by creating synthetic variables known as principal components (PC) that summarize the variance in the original data. The first PC is calculated such that it captures the largest portion of variance. The second PC is orthogonal to the first and captures the largest portion of the remaining variance. Each new PC is orthogonal to its preceding PCs and captures the largest portion of the remaining variance. Typically, only the first two or three PC dimensions are displayed in a figure as they sufficiently represent much of the variation within the entire dataset. In order to assess the clustering of biological replicates for each of the chosen normalization methods, PCA was performed on each of the normalized read datasets using Partek Flow (Partek Inc., St. Louis, MO, USA). Data was presented in two PC dimensions for ease of comparison between normalization methods.

III. RESULTS

In the following section, results are presented as upstream regulation of ΔNp63α by JNK (Section III.A) and the development and optimization of a suitable pipeline analysis for miRNA sequencing data to identify novel ΔNp63α-regulated miRNAs and pathways they affect (Section III.B).

A. Regulation of ΔNp63α by JNK kinase.

i. UVC and Anisomycin mediated JNK activation correlate with a ΔNp63α mobility shift

HaCaT cells were treated with either UVC (150 J/m^2) or Anisomycin (1 μg/ml), both potent inducers of stress activated protein kinases to confirm JNK activation. Cells were harvested at various time-points post treatment: 30 min, 1 hr, 2 hrs, and 4 hrs. Treatment with either UVC or Anisomycin led to a potent activation of JNK within 30 minutes of treatment (**Fig. 3A, B**). cJun, a downstream target of JNK, was also phosphorylated upon JNK activation within 30 minutes of treatment, serving as a positive control for JNK's kinase activity (**Fig. 3A, B**). Interestingly, we observed an electrophoretic mobility shift in the ΔNp63α specific band upon JNK activation as early as 30 min following UVC (**Fig. 3A**) and Anisomycin (**Fig. 3B**) treatment. This shift continued to increase through the 4-hour treatment. Our finding of UVC or Anisomycin induced electrophoretic mobility shift in ΔNp63α correlates with JNK activation, suggesting that JNK is likely responsible for the phosphorylation of ΔNp63α.

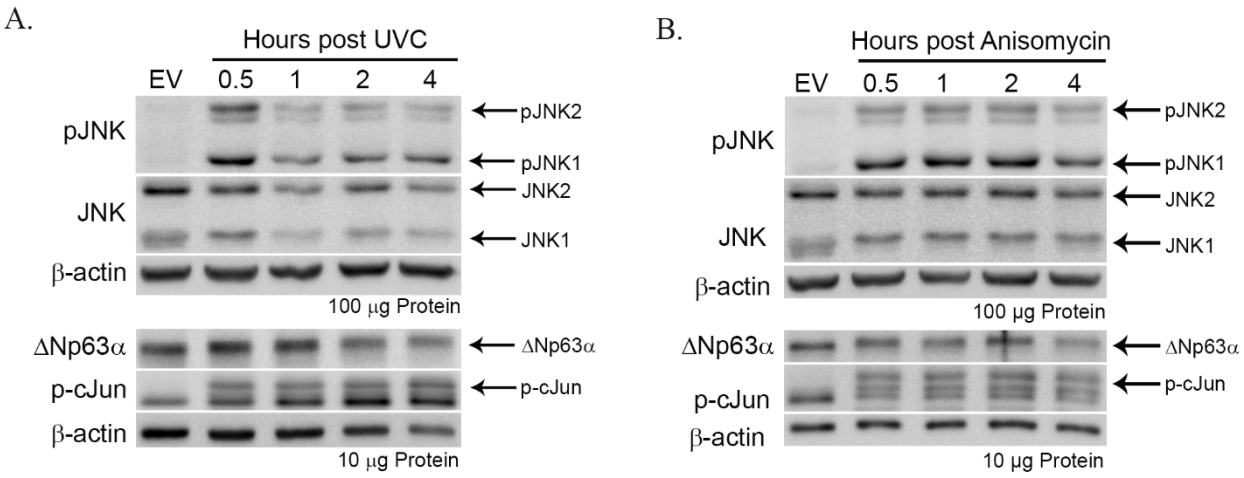

Figure 3: UVC and Anisomycin-induced JNK activation corresponds to an electrophoretic mobility shift in ΔNp63α. (A) HaCaT cells were treated with UVC (150 J/m^2) or (B) Anisomycin (1 μg/ml) or an equivalent volume of DMSO. Cells were harvested at various time-points post treatment and whole cell extracts were obtained. Protein extracts were subjected to immunoblot analysis for the phospho-JNK (pJNK), JNK, ΔNp63α, phospho-cJun (p-cJun), and β-actin. β-actin was included as a loading control to show an equivalent amount of protein was added in each lane.

ii. Co-Expression of ΔNp63α and JNK1/2 enhances the ΔNp63α mobility shift

We overexpressed ΔNp63α plasmid alone or with HA tagged JNK1 or JNK2 plasmid in H1299 cells, a non-small cell lung carcinoma cell line which is null for p53 and does not express p63. In the absence of UVC treatment, co-expression of JNK1 or JNK2 with ΔNp63α did not lead to a ΔNp63α electrophoretic mobility shift (**Fig. 4**). As expected, UVC treatment led to JNK activation when compared to untreated cells (**Fig. 4**), (compare lanes 9 – 12 to lanes 3 – 6) which corresponded to phosphorylation of its downstream target, c-Jun. Consistent with **Figure 1**, JNK activation corresponded to an electrophoretic mobility shift in ΔNp63α (**Fig. 4**, lanes 9 & 10) when compared to untreated cells (**Fig. 4**, lanes 3 & 4). These data are consistent with our hypothesis that JNK phosphorylates ΔNp63α.

iii. *in Vitro* Kinase Assay confirms that JNK directly phosphorylates ΔNp63α

In order to confirm that JNK1 and JNK2 are directly involved in the phosphorylation of ΔNp63α, an *in vitro* kinase assay was performed using recombinant ΔNp63α alone as a control or along with recombinant active JNK1 or JNK2 using ^{32}P γ-labeled ATP. In the Coomassie stain shown in **Figure 5**, the upper band represents the recombinant ΔNp63α and the lower band represents cleaved GST (residual contamination from the recombinant ΔNp63α protein purification). An autoradiograph of the dried gel clearly demonstrates that JNK1 and, to a lesser extent, JNK2 directly phosphorylate ΔNp63α. The lack of a GST tag band on the autoradiograph (**Fig. 5**, right panel) serves as an internal control indicating that phosphorylation of ΔNp63α by JNK1 and JNK2 was specific. Taken together, these results strongly suggest that JNK phosphorylates ΔNp63α as indicated by the mobility shift observed in **Figures 1** and **2**.

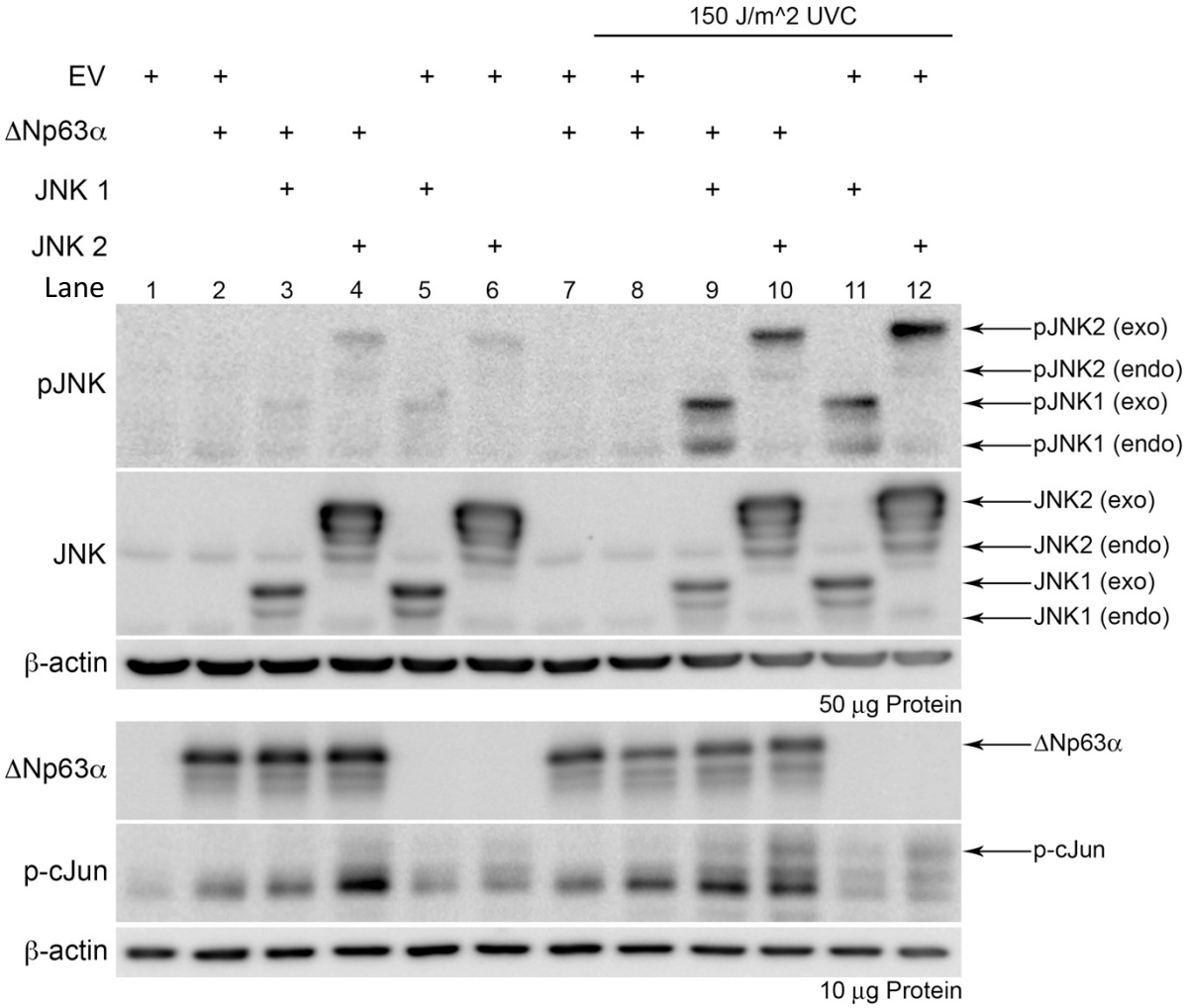

Figure 4: Co-expression of JNK and ΔNp63α leads to an enhanced mobility shift in ΔNp63α. H1299 cells were transfected with plasmids encoding either empty vector (EV), ΔNp63α (p63), HA-tagged JNK1, or HA-tagged JNK2 as indicated. Cells were treated with UVC (150 J/m^2) 24 hours post transfection and incubated in normal complete growth media for 2 hours following UVC treatment. Whole cell extracts were obtained. Protein extracts were subjected to immunoblot analysis for phospho-JNK (pJNK), JNK, ΔNp63α, phospho-cJun (p-cJun), and β-actin. β-actin was included as a loading control to show an equivalent amount of protein was added in each lane.

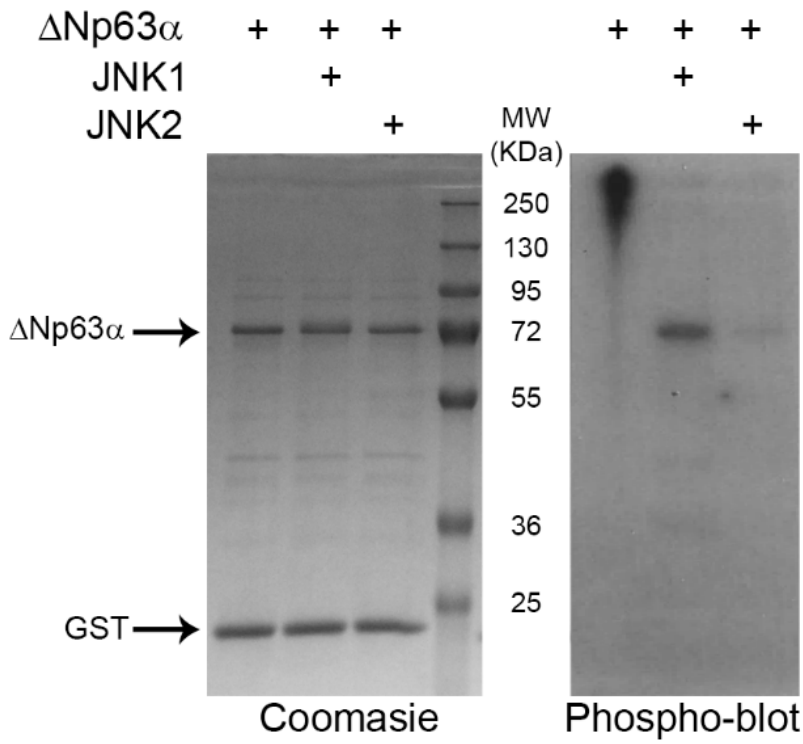

Figure 5: JNK phosphorylates ΔNp63α *in vitro*. Recombinant ΔNp63α and recombinant active JNK1 or JNK2 were incubated together in an *in vitro* kinase assay using ^{32}P γ-labeled ATP and subjected to SDS-PAGE. Recombinant proteins were Coomassie stained (Left) and analyzed for radiolabeled phosphorylation as shown in the autoradiograph (Right). Performed with the help of Dr. Weiwen Long at Wright State University.

iv. ΔNp63α is phosphorylated on conserved JNK-targeted residues

p63 is homologous to its family members p53 and p73 (Yang, Kaghad et al. 2002). Previously, p73 has been shown to be phosphorylated by JNK (Jones, 2007). As shown in **Figure 6**, both the JNK binding site as well as the p73 residues phosphorylated by JNK are highly conserved in human and mouse p63. It is known that ΔNp63α is phosphorylated *in vivo* by p38 in response to UV irradiation, while the ΔNp63γ isoform of p63 which lacks the C-terminal SAM and TID domains is not, suggesting that the region targeted by p38 lies within exons 11 and 12, specifically between amino acid residues 357 and 457 of ΔNp63α (Papoutsaki, Moretti et al. 2005). These are different from the predicted JNK target sites.

In order to identify potential JNK phosphorylation sites on ΔNp63α**,** whole cell extracts from UVC-treated H1299 cells expressing ΔNp63α were subjected to immunoprecipitation (IP) using a p63 specific antibody and subjected to SDS-PAGE analysis followed by Coomassie staining and immunoblot analysis. Recombinant GST-cleaved ΔNp63α was used as a marker for the immunoprecipitated ΔNp63α (approximately 72 kDa) (**Fig. 7A**). Immunoblot analysis confirmed an electrophoretic mobility shift in ΔNp63α (**Fig. 7B**). The ΔNp63α band was excised and subjected to mass spectrometry analysis. Post-translational modifications on ΔNp63α following UVC treatment were detected, revealing phosphorylation of multiple residues, three of which are conserved between p63 and p73 (**Fig 7C, D**).

v. Site directed mutagenesis of ΔNp63α

The mass spectrometry data along with the conservation of potential JNK phosphorylation residues, identified by comparison to p73, led us to focus on several residues as potential JNK

Figure 6: ΔNp63α contains putative JNK phosphorylation sites. JNK phosphorylation and interaction sites are conserved between p63 and p73. Aligned amino acid sequences of human and mouse ΔNp63α with human TAp73 are shown with the JNK interaction sequence (underlined) and putative phosphorylation sites, with the neighboring proline, in bold.

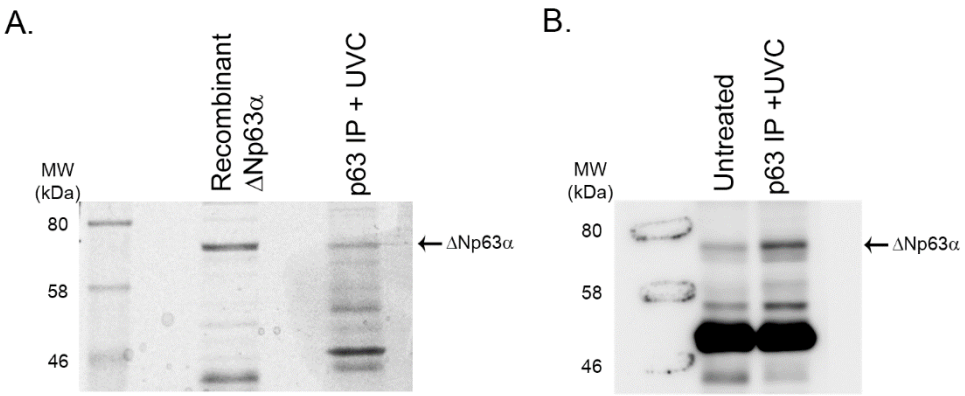

C.

UVC2: Sequence Coverage and prediction of PTM sites

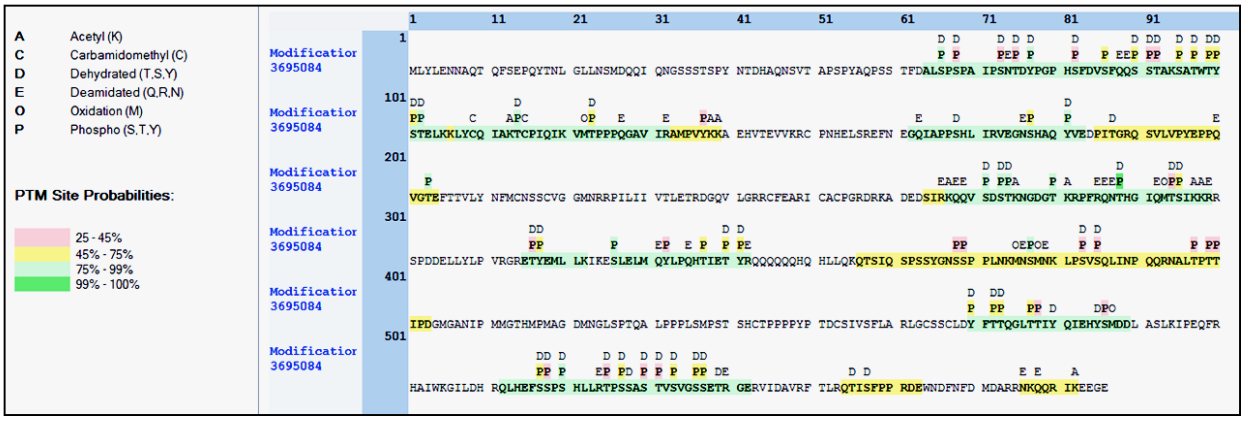

D.

Position	Target	Modification	Highest PTM Score	Highest Peptide Confidence	Sequence Motif
53	S	not detected			
66	S	Dehydrated		Middle	STFDALsPSPAI
66	**S**	**Phospho**	83.9	Middle	STFDALsPSPAI
369	**S**	**Phospho**	34.4	Middle	SSYGNSsPPLNK
397	**T**	**Phospho**	34.8	Middle	QQRNALtPTTIP
444	T	not detected			

Figure 7: Mass spectrometry data reveals potential sites of phosphorylation on ΔNp63α. H1299 cells were transfected with plasmid encoding ΔNp63α, treated with 150 J/m^2 UVC and maintained in complete media for 2 hours. Cells were harvested and subjected to immunoprecipitation with a pan-p63 antibody. Immunoprecipitated protein was subjected to (A) Coomassie stain and (B) immunoblot analysis to detect ΔNp63α. (C) The ΔNp63α band was excised from the Coomassie stained gel and subjected to mass spectrometry analysis to detect post-translational modifications. Phosphorylated residues are indicated as "P" with shading indicative of PTM site probability. (D) Phosphorylated ΔNp63α residues identified by mass spectrophotometry and homology to TAp73α are listed.

phosphorylation sites within ΔNp63α. To identify the significance of each of these potential sites, single phospho-deficient site mutants were constructed at S53, S66, S369, T397, and T444 by mutating the wild type residues into an alanine (**Table 1**). We examined whether these sites are required for the phosphorylation of ΔNp63α by UV-activated JNK. H1299 cells were transfected with wild type ΔNp63α or the single phospho-deficient site mutants and treated with UVC.

UVC treatment resulted in the activation of JNK1 and JNK2 as expected and the phosphorylation of its downstream substrate c-Jun (**Fig. 8A**), consistent with Figures 1 and 2. Furthermore, wild-type ΔNp63α exhibited an electrophoretic mobility shift upon UVC treatment as expected (**Fig. 8A**). However, the single phospho-deficient site mutants also exhibited an electrophoretic mobility shift similar to that observed in wild-type ΔNp63α following UVC treatment (**Fig. 8A**), suggesting loss of any of the single phosphorylation sites was insufficient to fully block UVC-mediated phosphorylation of ΔNp63α by JNK. To determine whether the electrophoretic mobility shift in exogenously supplied ΔNp63α could be enhanced by increasing active JNK levels, H1299 cells were co-transfected with ΔNp63α and HA tagged JNK1 or JNK2 or the single phospho-deficient site mutants and HA tagged JNK1 or JNK2 followed by UVC treatment (**Fig. 8B, C**). Wild-type ΔNp63α co-expressed with JNK1 and JNK2 exhibited an electrophoretic mobility shift upon UVC treatment, as expected (**Fig. 8B, C**). Similarly, the UVC-induced electrophoretic mobility shift of the single phospho-deficient site mutants was enhanced when overexpressed with JNK1 or JNK2 (**Fig. 8B, C**). The observation that the electrophoretic mobility shift was unchanged in the single phospho-deficient ΔNp63α mutants suggests either that multiple residues on ΔNp63α may be phosphorylated by JNK, or that another residue not tested is responsible for the observed mobility shift.

ΔNp63α		
Position	Wild Type	Mutant
53	S	A
66	S	A
369	S	A
397	T	A
444	T	A

Table 1: Site directed mutagenesis of ΔNp63α. Five (S53A, S66A, S369A, T397A, T444A) single phospho-deficient mutants of ΔNp63α were synthesized by replacing the wild type amino acid residue with an alanine. A multiple phospho-deficient mutant of ΔNp63α (all seven amino acid residues mutated) was synthesized by replacing the wild type amino acid residues with alanine.

A.

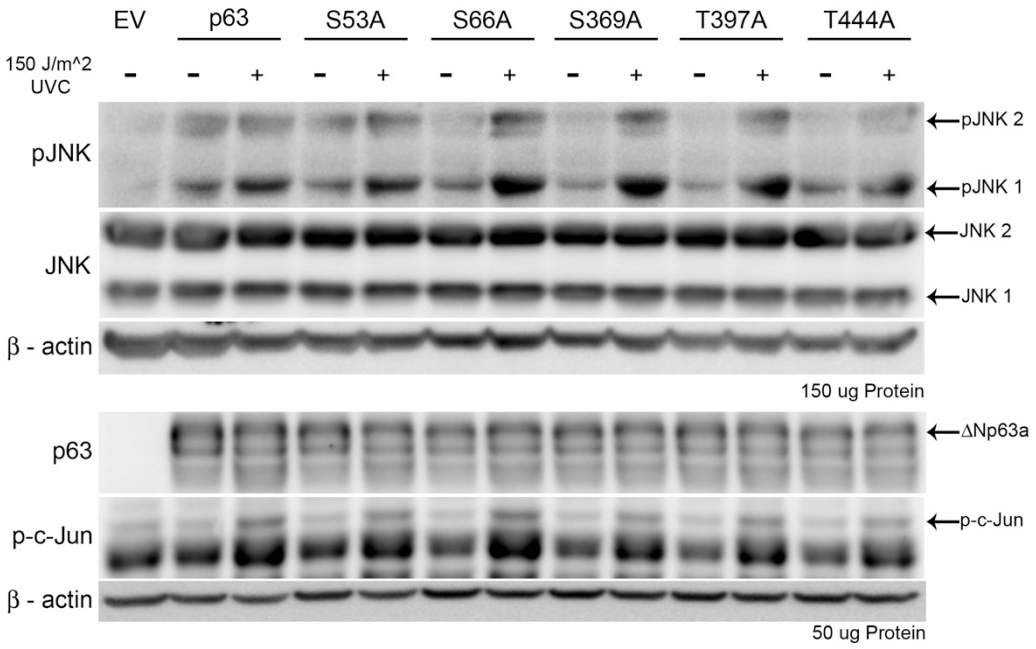
EV
p63
S53A
S66A
S369A
T397A
T444A
150 J/m^2 UVC
- - + - + - + - + - + - +
pJNK
pJNK 2
pJNK 1
JNK
JNK 2
JNK 1
β - actin
150 ug Protein
p63
ΔNp63a
p-c-Jun
p-c-Jun
β - actin
50 ug Protein

B.

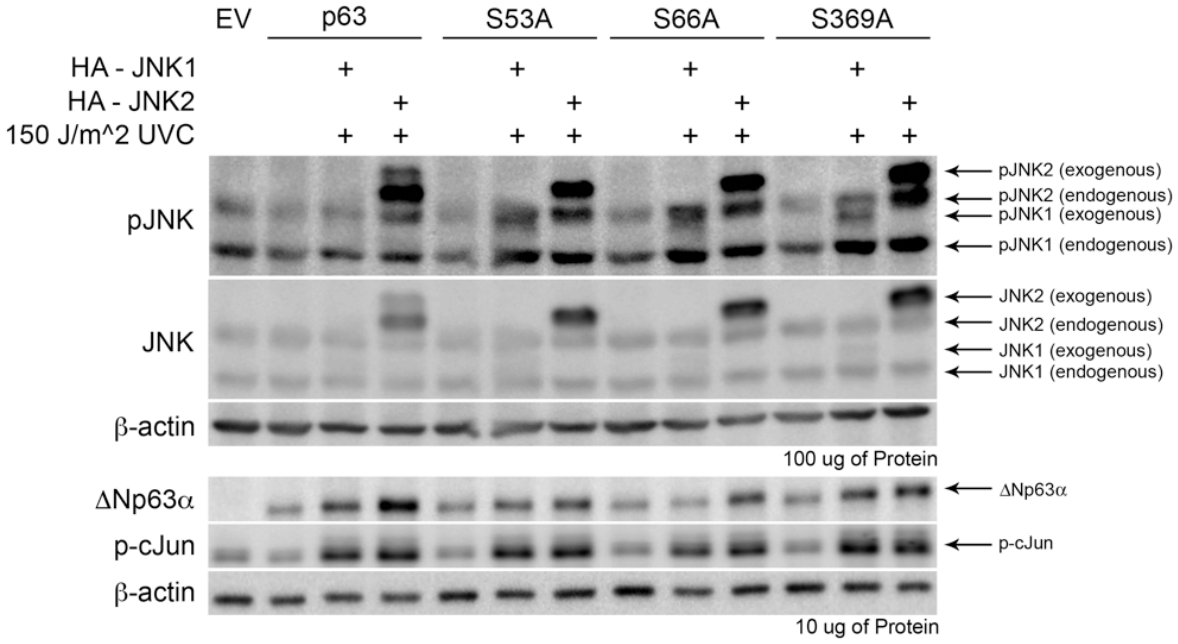
EV
p63
S53A
S66A
S369A
HA - JNK1
HA - JNK2
150 J/m^2 UVC
pJNK
pJNK2 (exogenous)
pJNK2 (endogenous)
pJNK1 (exogenous)
pJNK1 (endogenous)
JNK
JNK2 (exogenous)
JNK2 (endogenous)
JNK1 (exogenous)
JNK1 (endogenous)
β-actin
100 ug of Protein
ΔNp63α
ΔNp63α
p-cJun
p-cJun
β-actin
10 ug of Protein

C.

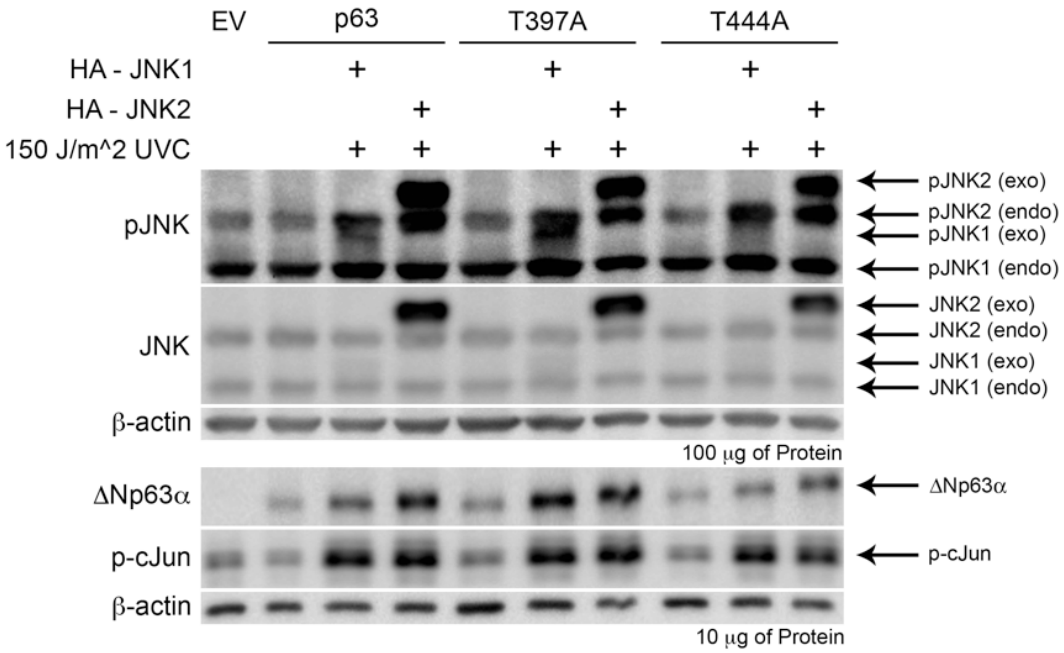

Figure 8: Mutation of single phosphorylation sites of ΔNp63α does not prevent its mobility shift. (A) H1299 cells were transfected with empty vector, myc-tagged wild type ΔNp63α, S53A, S66A, S369A, T397A, and T444A ΔNp63α mutants. 24 hrs post transfection, cells were treated or left untreated with UVC (150 J/m^2). Protein lysates were subjected to immunoblot analysis. **(B)** H1299 cells were transfected with empty vector, myc-tagged wild type ΔNp63α or a multiple phospho-deficient ΔNp63α mutant. Cells were then treated with UVC (150 J/m^2) or Anisomycin (1 μg/ml). Protein lysates were subjected to immunoblot analysis. β-actin was included as a loading control to show an equivalent amount of protein was added in each lane.

In order to identify additional candidate phosphorylation sites, an *in vitro* kinase assay using recombinant ΔNp63α in conjunction with recombinant active JNK1 or JNK2 in the presence of non-radiolabeled ATP was performed. These samples were subject to mass spectrometry analysis to reveal potential sites of phosphorylation (**Fig. 9**). Specifically, residues T288 and S361, were phosphorylated by both JNK1 and JNK2 making them potential sites to consider for mutagenesis.

In order to test the possibility that the observed mobility shift in ΔNp63α was caused by concurrent phosphorylation of multiple residues, a phospho-deficient mutant (PD mut) with all the site directed mutations identified by mass spectrometry was generated. Residues S53, S66, S361, S369, T288, T397, and T444 were mutated to an alanine to prevent phosphorylation at those sites and transfected into H1299 cells to test whether the mutant protein exhibited a UV-induced electrophoretic mobility shift. As shown previously, UVC treatment led to phosphorylation of c-Jun, confirming that JNK was activated despite detecting low levels of active JNK. That corresponded with a slight mobility shift in wild-type ΔNp63α (**Fig. 10**). H1299 cells transfected with the PD-mut and treated with UVC did result in a slight mobility shift as well. Interestingly, there was a significant decrease in protein levels of the wild-type ΔNp63α following UVC or Anisomycin treatment consistent with previous reports that phosphorylation of ΔNp63α targets it for ubiquitin-mediated degradation (Yang, Kaghad et al. 2002, Di Costanzo, Festa et al. 2009, Lazzari, Prodosmo et al. 2011). By contrast, however, the protein levels of the PD-mut remained largely unchanged following UVC or Anisomycin treatment compared to the wild-type (**Fig. 10**). This suggests that the mutation of these residues may prevent JNK-mediated phosphorylation and prevent tagging for proteasomal degradation, whereas, the wild-type is subject to JNK-mediated phosphorylation and subsequent targeting for proteasomal degradation.

ΔNp63α + JNK1

Position	Target	Modification	Classification	Highest PTM Score	Highest Peptide Confidence	Sequence Motif
168	S	Phospho	Post-translational	100	High	GQIAPPsHLIRVE
288	T	Phospho	Post-translational	76.1	High	RPFRQNtHGIQMT
294	T	Phospho	Post-translational	82	High	THGIQMtSIKKRR
361	S	Phospho	Post-translational	80.3	High	KQTSIQsPSSYGN

ΔNp63α + JNK2

Position	Target	Modification	Classification	Highest PTM Score	Highest Peptide Confidence	Sequence Motif
288	T	Phospho	Post-translational	100	High	RPFRQNtHGIQMT
332	Y	Phospho	Post-translational	94.7	High	SLELMQyLPQHTI
361	S	Phospho	Post-translational	65.2	High	KQTSIQsPSSYGN
520	S	Phospho	Post-translational	65.4	High	HEFSSPsHLLRTP

Figure 9: Sites on ΔNp63α that are highly phosphorylated in response to JNK. Sites were identified by mass spectrometry following an *in vitro* kinase assay utilizing non-radiolabeled ATP. (Top chart) Sites on ΔNp63α that are phosphorylated by recombinant active JNK 1. (Bottom chart) Sites on ΔNp63α that are phosphorylated by recombinant active JNK 2.

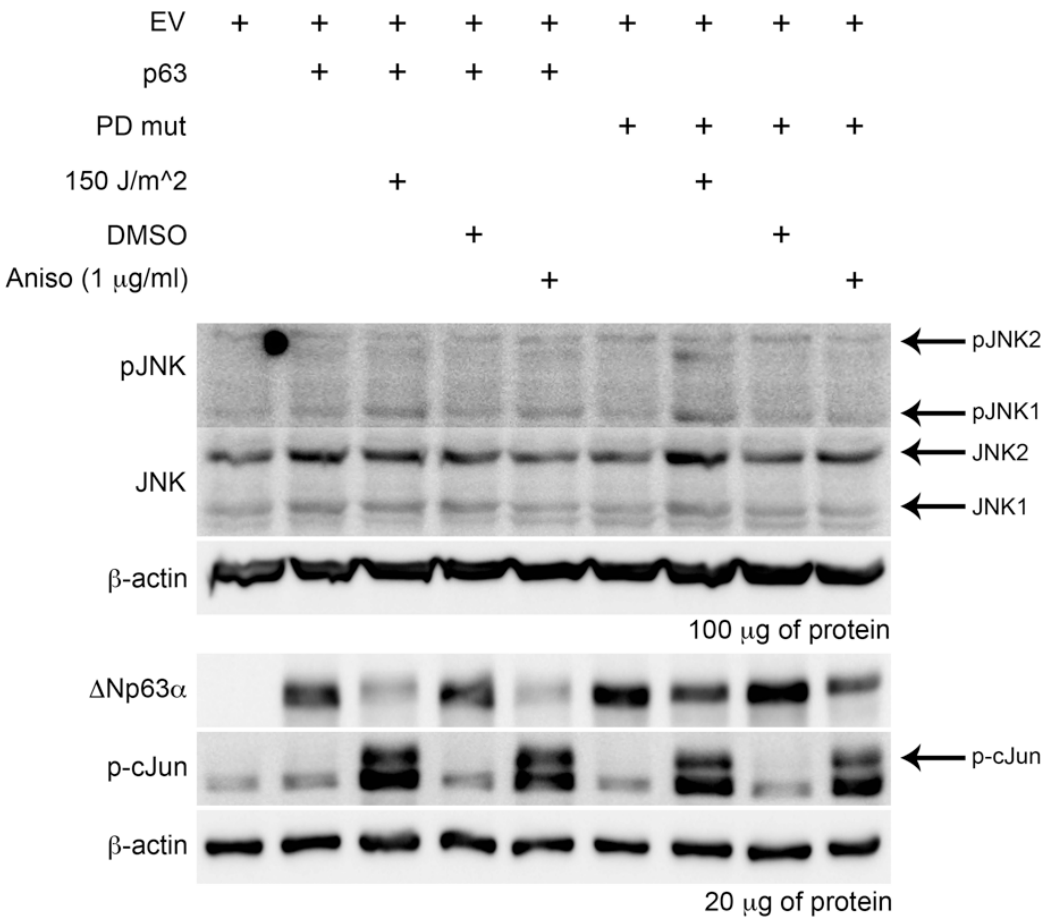

Figure 10: Site-directed mutagenesis of multiple phospho-residues attenuates protein degradation. H1299 cells were transfected with empty vector, myc-tagged wild type ΔNp63α or the multiple phospho-deficient ΔNp63α mutant (PD mut). Cells were then treated with UVC (150 J/m^2) or Anisomycin (1 μg/ml). Whole cell extracts were subjected to immunoblot analysis. β-actin was included as a loading control to show an equivalent amount of protein was added in each lane.

B. Identification of ΔNp63α targeted miRNA by small RNA-Seq by establishing an optimized small RNA-Seq pipeline

Currently, there is no consensus on a formal analysis pipeline for analyzing miRNA sequencing data. My goal was to develop an optimized pipeline workflow for analyzing miRNA sequencing data that would be accurate, stringent, and reliable, thus providing consistent results. The various alignment references, normalization methods, and response distribution models available for small RNA-Seq data processing affect the number of miRNAs that are classified as significantly differentially expressed, making the selection of optimal processing parameters critical for accurate miRNA expression profiling and validation (Langmead and Jha 2009, Oshlack, Robinson et al. 2010, Ramskold, Kavak et al. 2012, Conesa, Madrigal et al. 2016). I tested multiple analysis pipeline configurations including multiple permutations at crucial data processing steps while keeping the remaining processing parameters consistent. **Figure 11** shows an overview of the processing workflows considered in pipeline optimization analysis.

i. Silencing p63

HaCaTs, non-tumorigenic keratinocyte cells, were used to study ΔNp63α's role within epithelial tissue. These cells were chosen because they express ΔNp63α, the most physiologically relevant isoform of p63 expressed in the basal layer of the skin (Koster, Kim et al. 2004, Koster and Roop 2004, Koster and Roop 2004). All three biological replicates of HaCaT cells transfected with siRNA against p63 (sip63) showed an 80% reduction in p63 transcript levels (**Fig. 12A**) and no detectable p63 protein (**Fig. 12B**) relative to the non-silencing control (NSC) (representative data shown).

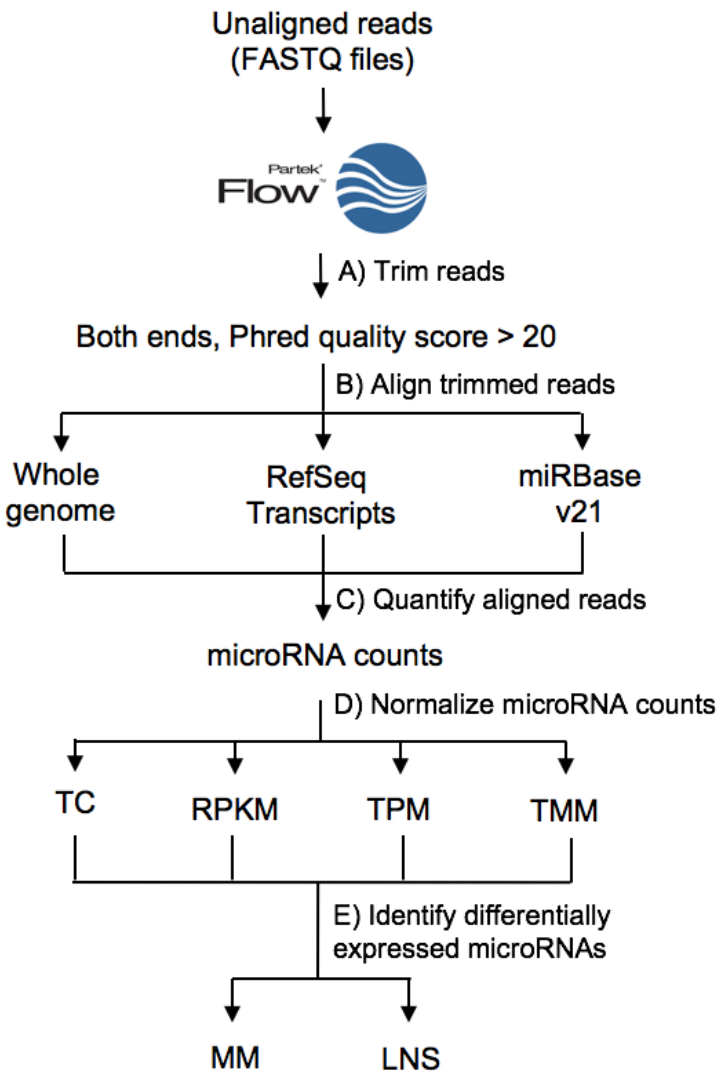

Figure 11: Data processing workflow. Schematic of workflow for evaluating different combinations of alignment references and normalization procedures considered in our studies.

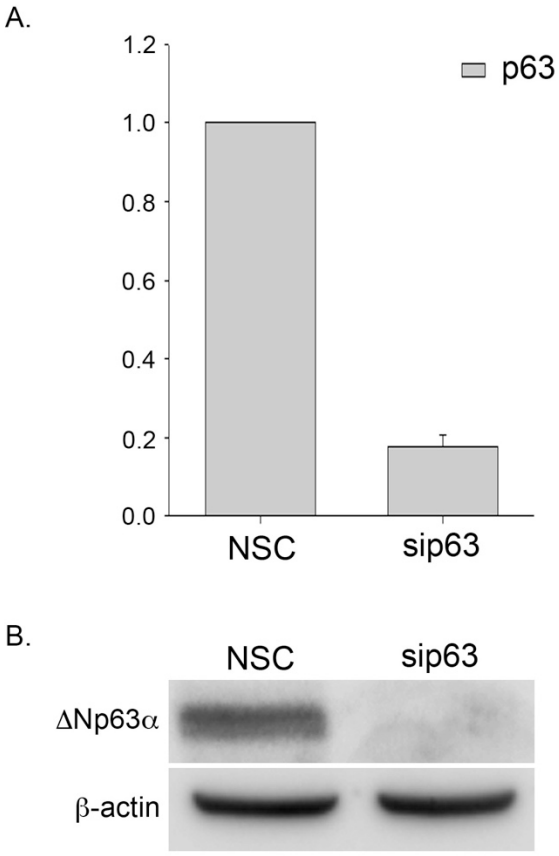

Figure 12: ΔNp63α is silenced in HaCaT samples used for small RNA-Seq. HaCaT cells were transfected with either non-silencing control siRNA or siRNA against p63. A) qRT-PCR analysis of p63 transcript levels normalized to endogenous GAPDH. B) p63 protein levels in NSC and sip63 cell lysates. β-actin was included as a loading control to show an equivalent amount of protein was added in each lane. Silencing experiments were performed and confirmed by Dr. Natasha T. Hill.

ii. Qualitative assessment of small RNA-Seq data

Unaligned reads were trimmed on both ends prior to the alignment step based on a Phred quality score of 20 and a minimum read length of 15 in order to capture the population of miRNAs in our samples. Quantitating the aligned reads from the HaCaT study samples yielded a raw read count for each miRNA feature in the miRBase database for each sample. I assessed the distribution of miRNA read counts obtained by whole genome, RefSeq, and miRBase aligned reads (**Fig. 13**). The distribution of the whole genome or RefSeq Transcripts aligned reads were very similar with most of miRNAs having 0 reads, indicating that approximately 85% of miRNA features were not quantified after aligning to either reference. By contrast, a majority of miRBase aligned reads had miRNAs with counts between 10 and 1,000 reads. Thus, more miRNA features were quantified with the aligned reads when miRBase was used as the alignment reference.

The quality of read mapping for each alignment was assessed by determining the percentage of aligned reads that mapped to actual miRNA sequences. **Table 2** summarizes the percent match and quantified reads for each of the alignment references. Aligning to whole genome and RefSeq Transcripts references yielded on average more mapped reads as compared to aligning to miRBase for both sip63 and NSC (**Table 2**). However, only a small fraction of those aligned reads mapped fully within a miRNA and were quantified as such. The opposite was the case with miRBase alignment reference. Although only a small percentage of total reads were mapped, 100% of the mapped reads were quantified as miRNA counts yielding on average more miRNA counts than whole genome and RefSeq Transcript aligned reads. Only 1 alignment was reported per read (the first valid alignment Bowtie comes across), suggesting that in aligning to the whole genome or RefSeq Transcripts, there was a higher probability for reporting an aligned read

A.

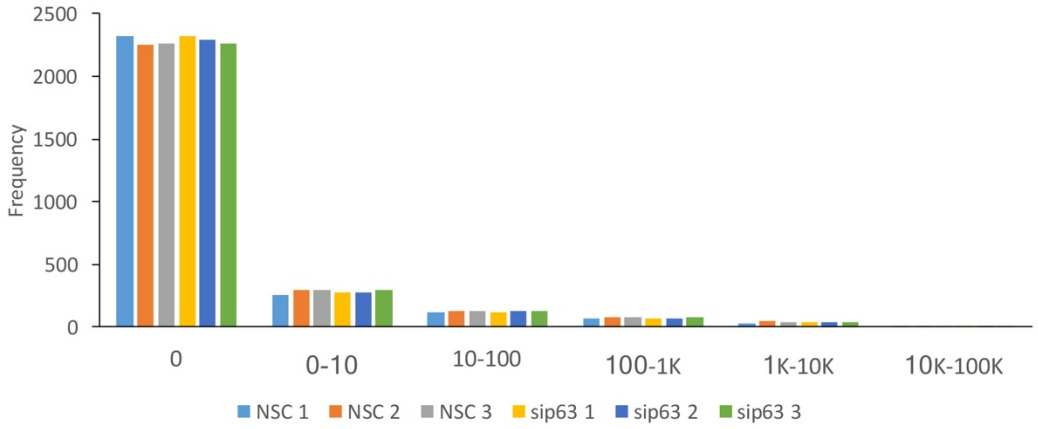
Whole genome aligned
2500
2000
1500
1000
500
0
Frequency
0
0-10
10-100
100-1K
1K-10K
10K-100K
NSC 1
NSC 2
NSC 3
sip63 1
sip63 2
sip63 3

B.

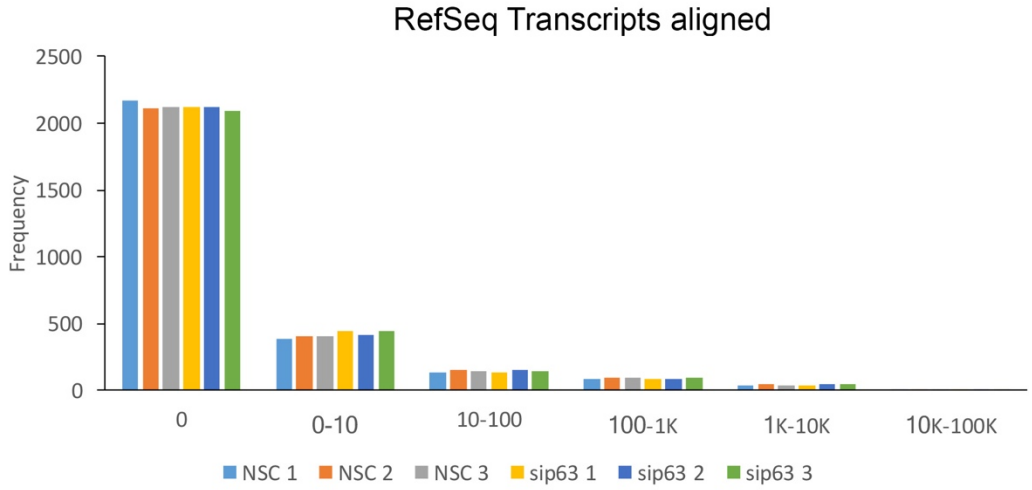
RefSeq Transcripts aligned
2500
2000
1500
1000
500
0
Frequency
0
0-10
10-100
100-1K
1K-10K
10K-100K
NSC 1
NSC 2
NSC 3
sip63 1
sip63 2
sip63 3

C.

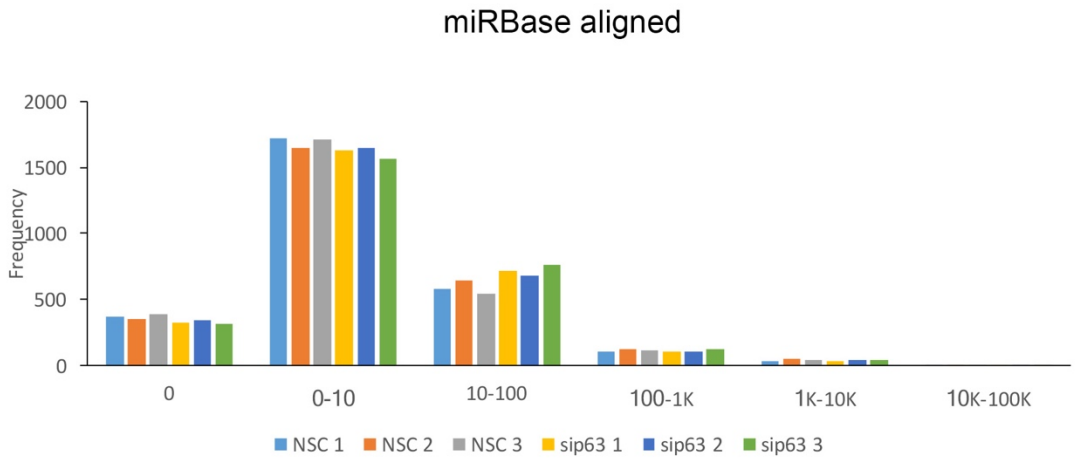
miRBase aligned
2000
1500
1000
500
0
Frequency
0
0-10
10-100
100-1K
1K-10K
10K-100K
NSC 1
NSC 2
NSC 3
sip63 1
sip63 2
sip63 3

Figure 13: Raw read count distributions for each alignment reference. The frequency of raw read counts from each of the biological replicates for each of the datasets (NSC and sip63) is shown for (A) WG, (B) RefSeq and (C) miRBase. Alignments were made with a 1 mismatch allowance.

Table 2: Effect of alignment reference on read quantification.

	Sample	Avg Aligned Reads (X1000)	Avg Fully within microRNA (%)	Avg microRNA counts (X1000)
Whole Genome	NSC	1828 +/- 427	14.9 +/- 0.02	273 +/- 68
	sip63	1723 +/- 158	11.4 +/- 0.00	197 +/- 20
RefSeq Transcripts (05-02-2016)	NSC	1375 +/- 291	21.6 +/- 0.02	297 +/- 73
	sip63	1301 +/- 159	17.0 +/- 0.00	220 +/- 23
miRBase mature microRNAs v21	NSC	341 +/- 80	100 +/- 0.00	341 +/- 80
	sip63	263 +/- 26	100 +/- 0.00	263 +/- 26

that did not correspond to a miRNA sequence, decreasing the chances of quantifying true miRNAs, thus increasing the false negative rate for quantification. For this reason, the miRBase reference was selected as the best reference to use for alignment.

In order to determine the optimal normalization method for our miRNA sequencing datasets, miRNA read counts were normalized using each of four normalization methods: RPKM, TPM, TC, and TMM. **Table 3** lists the major differences between the chosen methods. To compare the effect of each of the normalization methods on the dataset, miRNA with read counts greater than or equal to 10 reads (recommended by Partek as a low expression threshold) were log-transformed and the distribution between the raw and normalized reads datasets were assessed using boxplots for each of the various alignment references (**Fig. 14-16**). The raw read count dataset showed variation in the minimum, maximum and median values across conditional replicates (**Fig. 14-16**), reflecting the differences in sample size and composition across the replicates such as highly expressed miRNAs or a high amount of lowly expressed miRNAs that would affect the calculation of scaling factors, an artifact that is inherently present in the distribution of the datasets.

I evaluated the normalization methods' effectiveness based on how well each method stabilized the median distribution after the normalization. Stabilization of the median distribution indicates that majority of the miRNAs from each of the replicates have similar expression values adhering to the underlying assumption that most miRNAs are not differentially expressed. For whole genome (**Fig. 14**) and RefSeq Transcripts (**Fig. 15**) aligned reads, each normalization method stabilized values at their minima, where all the minima values are equal. With regards to the median distribution, compared to the raw reads, each of the normalization methods remove some of the variation present in the samples, particularly for the sip63 samples, however RPKM

Table 3: Normalization method comparison.

Normalization Method	Normalize for gene length?	Normalize for read depth?	Compare across samples?	Assume most genes are non-DE?
TMM	No	Yes	Yes	Yes
TC	No	Yes	No	No
RPKM	Yes	Yes	No	No
TPM	Yes	Yes	Yes	No

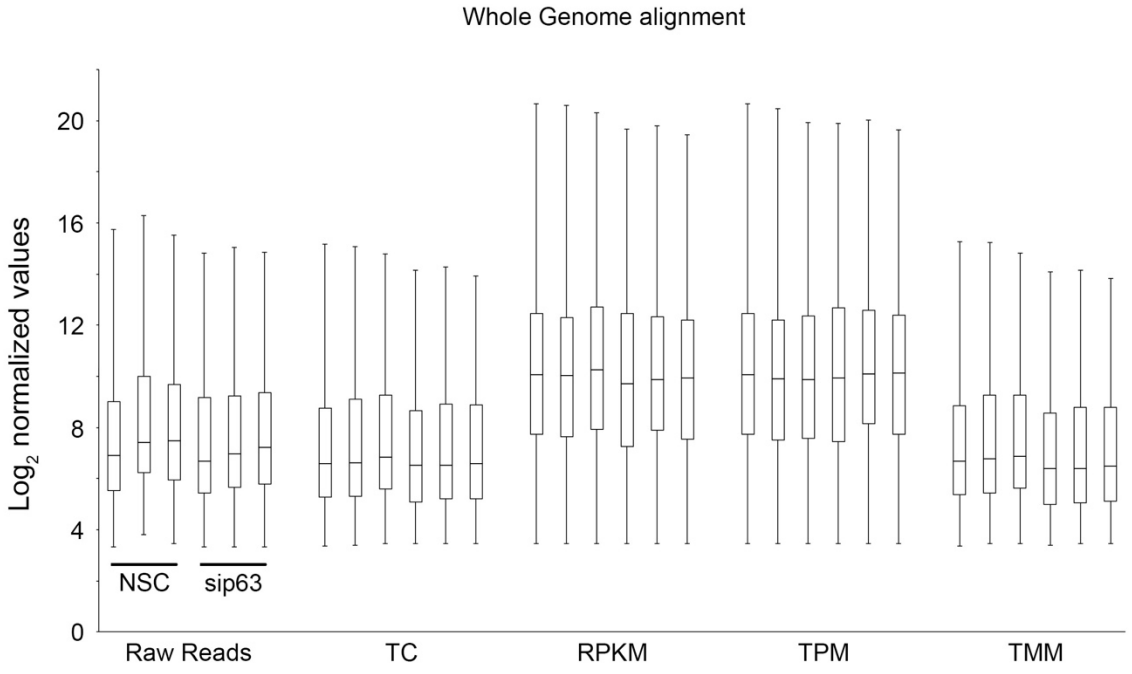

Figure 14: Effect of normalization method on the distribution of Whole Genome aligned reads. Log expression of miRNAs with reads greater than 10 in every sample are shown. For every normalization method, the first set of three bars represent NSC replicates 1, 2, and 3 and the second set of three bars represent sip63 replicates 1, 2, and 3.

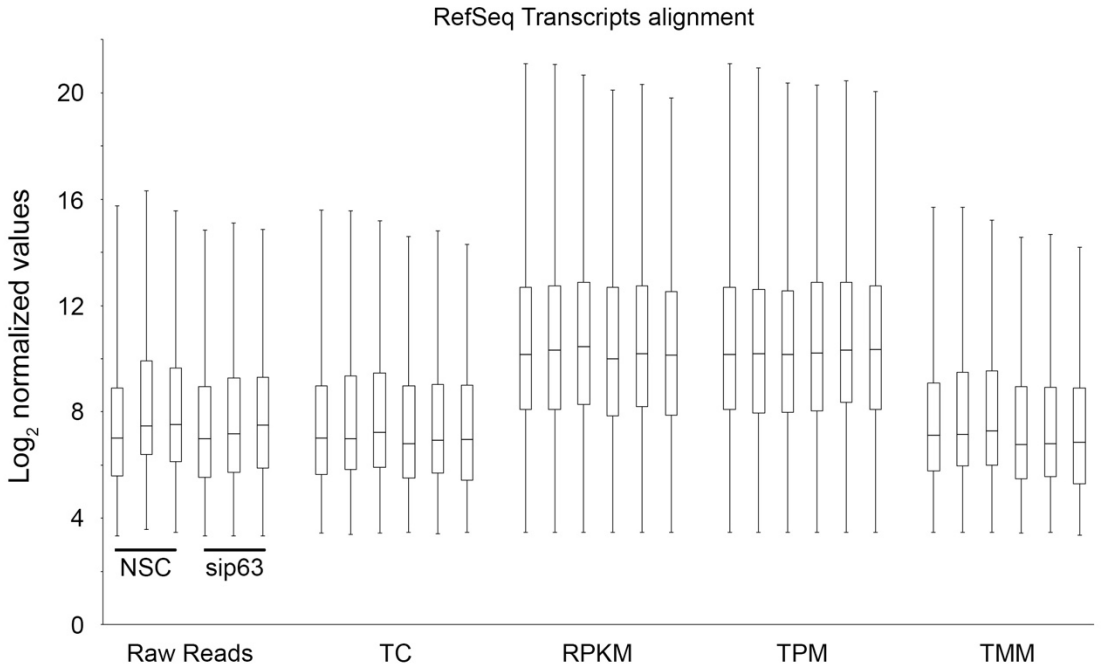

Figure 15: Effect of normalization on the distribution for RefSeq aligned reads. Log expression of miRNAs with reads greater than 10 in every sample are shown. For every normalization method, the first set of three bars represent NSC replicates 1, 2, and 3 and the second set of three bars represent sip63 replicates 1, 2, and 3.

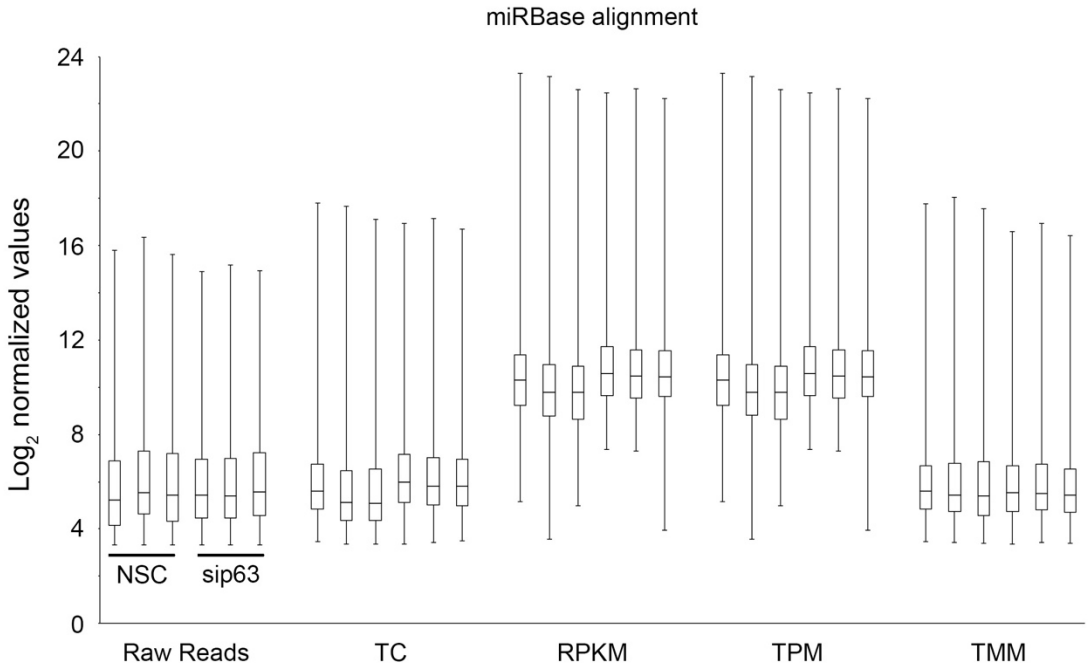

Figure 16: Effect of normalization methods on the distribution of miRBase aligned reads. Log expression of miRNAs with reads greater than 10 in every sample are shown. For every normalization method, the first set of three bars represent NSC replicates 1, 2, and 3 and the second set of three bars represent sip63 replicates 1, 2, and 3.

and TPM normalizations increased the spread of the data, which would potentially affect downstream differential expression analysis. Between the four normalizations, TC and TMM showed stabilization of their median values within conditional replicates without increasing the overall spread of the distribution such as the effect of RPKM and TPM normalization. Irrespective of which alignment reference was used, RPKM and TPM normalized distributions were similar to each other, as expected, because TPM is a modified version of RPKM. By contrast, miRBase aligned reads (**Fig. 16**) exhibited a different distribution pattern, possibly due to more miRNAs being quantified. TC, RPKM, and TPM all had poor stabilization of the median values compared to the raw read counts, whereas TMM showed stabilization not just within the replicates, but across all 6 samples. Overall, it should be noted that miRBase aligned reads had a more compact interquartile range suggesting that the miRBase aligned dataset had a smaller variation in frequency of miRNA counts for each miRNA than compared to whole genome or RefSeq Transcripts aligned reads, suggesting that the miRBase alignment reference provides an advantage in accurately quantifying mapped reads, which in turn improves the accuracy of the downstream differential expression analysis.

I compared the effect of each normalization method using Principal Components Analysis (PCA). PCA plots for each normalization method are displayed in two principal component dimensions for ease of comparison between each of the normalization methods. **Figure 17** displays PCA plots for each normalization method from the whole genome aligned reads. Similarly, **Figures 18** and **19** display PCA plots for each normalization method from the RefSeq aligned reads and miRBase aligned reads, respectively. In every PCA plot of normalized data, I expected to see a clustering of replicates within their respective conditional groups, suggesting that normalization could group replicates together in an unsupervised manner. All the normalization

methods except TPM showed a clear separation of the replicate groups as compared to the raw reads (pre-normalization) (**Fig. 17-19**). Regardless of which alignment reference was used, TMM normalization showed the greatest degree of separation between the conditional groups (**Fig. 17-19**).

iii. Differential Expression Analysis

I performed differential expression analysis between sip63 and NSC replicates in order to identify miRNAs that are differentially regulated by ΔNp63α. I tested two different approaches to model our data: the multimodel approach and lognormal with shrinkage (LNS) approach (detailed in the materials and methods). The major difference between the two approaches is that multimodel chooses the response distribution model that best fits miRNA expression levels across the replicates. While this seems to provide the best description of a given miRNA's expression pattern, it does not necessarily translate to the underlying trend in the population and can potentially over fit the data. LNS, however, ensures higher reproducibility in obtaining similar results based on pooling variance information across all genes, resulting in a higher, more reproducible study, especially under low replicate experiments. This is similar to the "limma trend" method from the limma package (Law, Chen et al. 2014). With any given RNA-Seq experiment, it is important to account for two main sources of variation: technical variation, a measure of error inherent to the sequencing technology and sample preparation, and biological variation, a representation of the heterogeneity among samples in similar treatment groups (Wu, Wang et al. 2013). I reasoned that the appropriate model would be one which accounts for the effect of gene-specific dispersion. The LNS approach uses an empirical Bayes method that better estimates gene-specific dispersion by

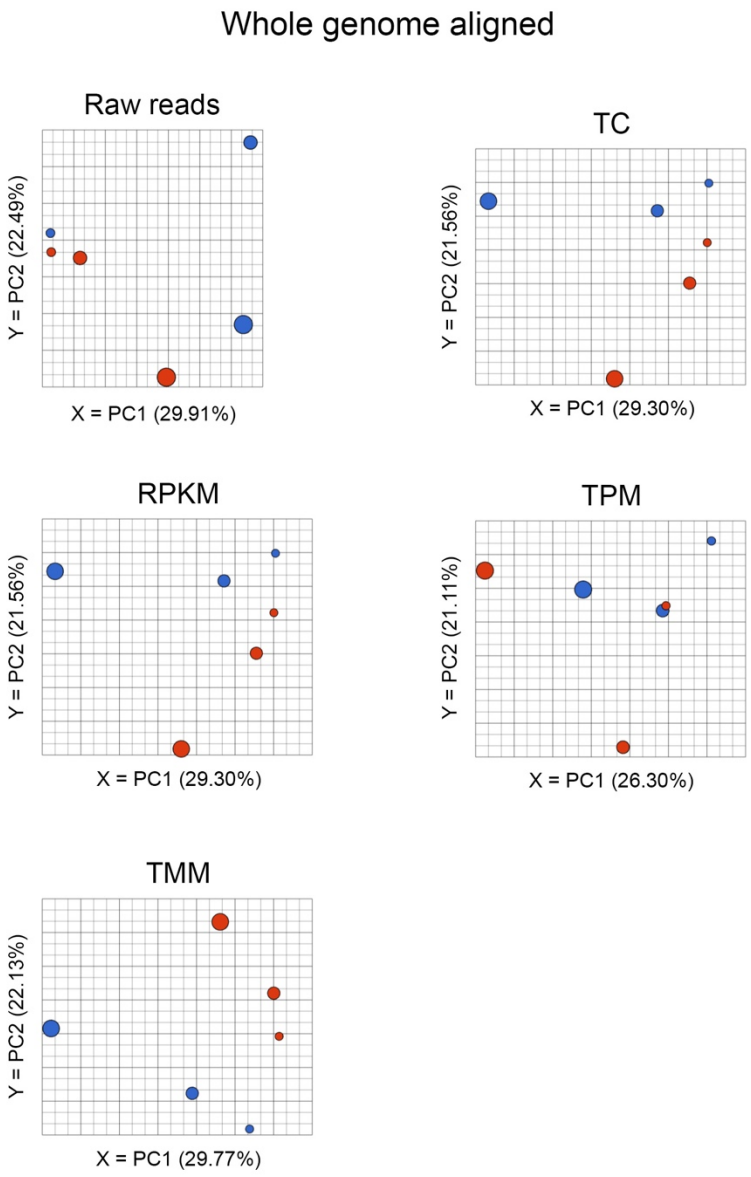

Figure 17: Principal component analysis of whole genome aligned samples before and after normalization. Variation in dot size corresponds to the biological replicate. Blue dots denote NSC samples and red dots denote sip63 samples.

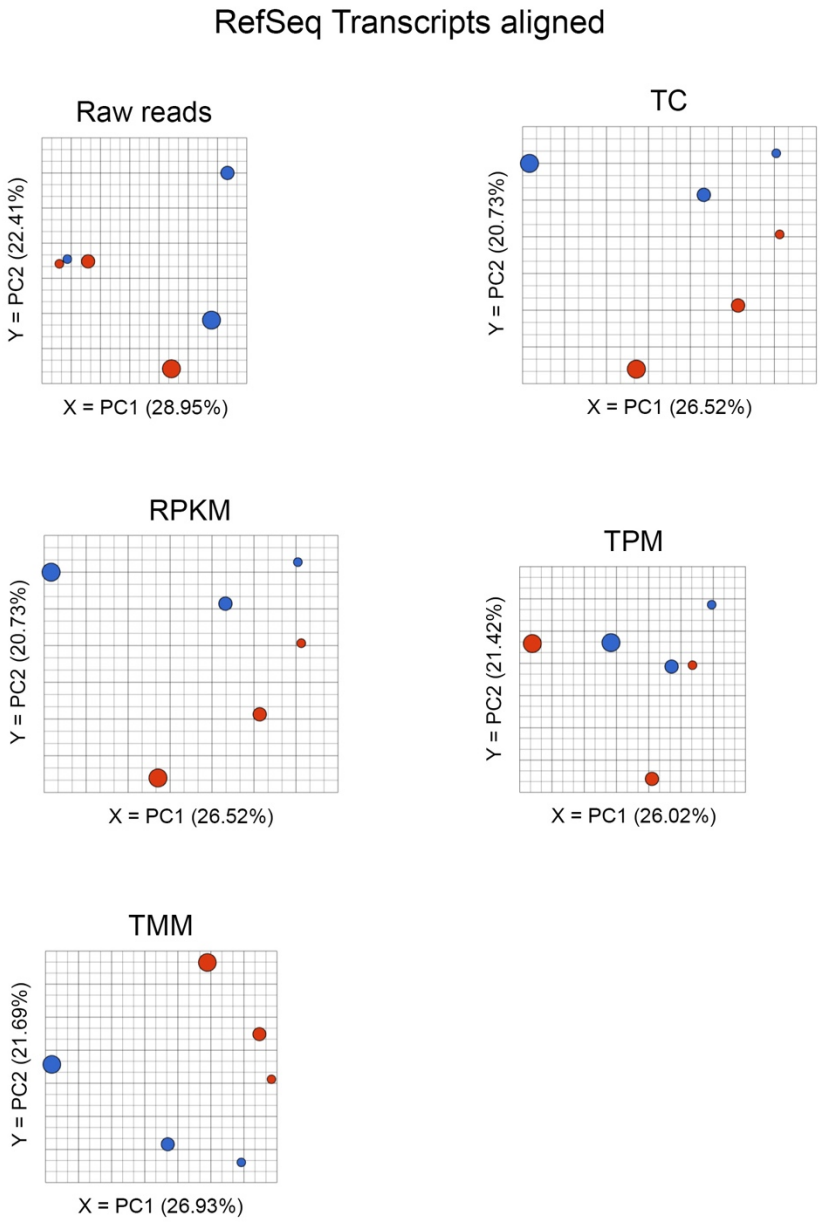

Figure 18: Principal component analysis of RefSeq aligned samples before and after normalization. Variation in dot size corresponds to the biological replicate. Blue dots denote NSC samples and red dots denote sip63 samples.

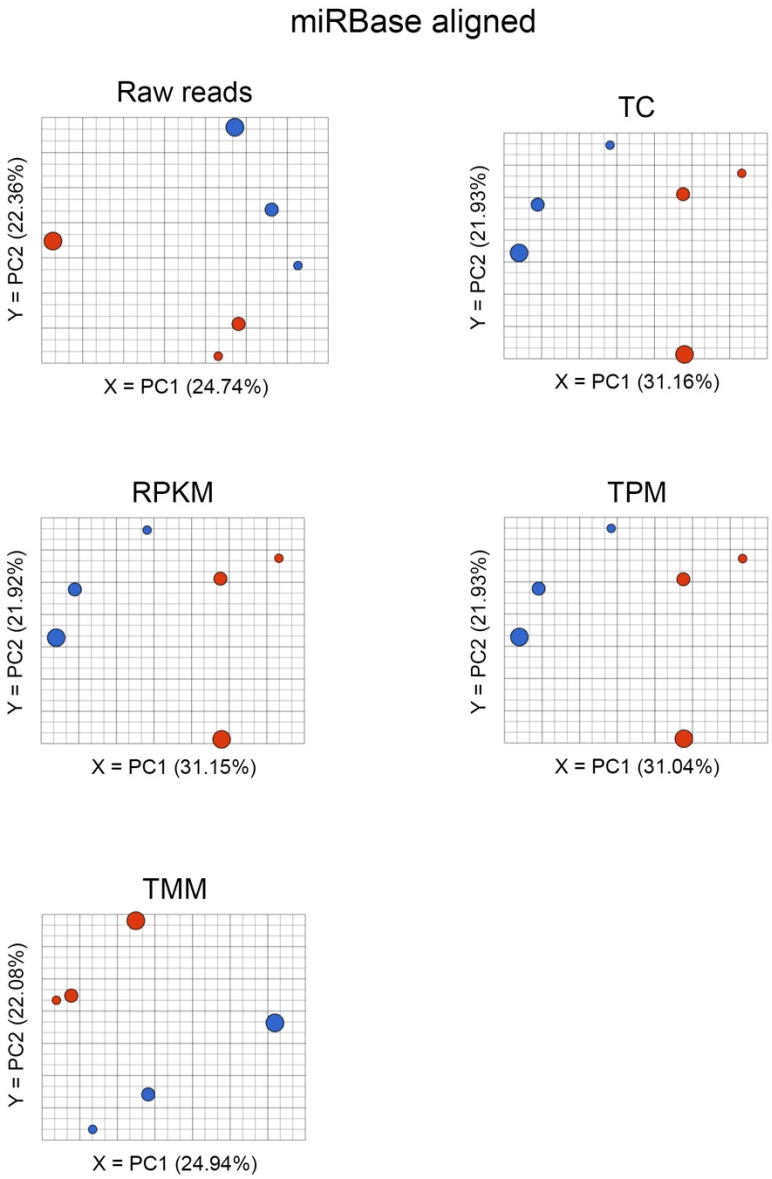

Figure 19: Principal component analysis of miRBase aligned samples before and after normalization. Variation in dot size corresponds to the biological replicate. Blue dots denote NSC samples and red dots denote sip63 samples.

combining information about variance from other genes to improve the estimation process, resulting in improved DE detection and lower false-positive rates (Wu, Wang et al. 2013). I chose lognormal with shrinkage as the best response distribution as it accounts for the effect of gene-specific dispersion in an experiment, thus improving reproducibility across multiple experiments.

Tables 4 and 5 show the number of significantly differentially expressed miRNAs based on the alignment reference and normalization method used for both approaches. Similar to the box-plot distribution comparisons, whole genome and RefSeq Transcripts aligned datasets yielded a similar number of miRNAs that were considered to be significantly differentially expressed, while miRBase aligned reads had a considerably higher number of miRNA that are deemed significantly differentially expressed. This suggests that mapping to whole genome and RefSeq Transcripts references results in a large portion of low expressed miRNAs being filtered during the quantification step that would otherwise have information regarding its differential expression. There were subtle differences in the number of miRNAs that were significantly differentially expressed between multimodel and LNS approach for the whole genome and RefSeq transcripts alignment references, wherein the significant DE miRNAs from LNS were a subset of the significant DE miRNAs from multimodel.

I specifically considered the list of significantly differentially expressed miRNAs obtained from aligning to miRBase and normalizing miRNA counts using TMM from the LNS approach and assessed the overall performance of that pipeline. **Figure 20** shows a heat map clustered by sample and feature using a Euclidean distance metric and average clustering metric for the 191 differentially expressed miRNAs that were identified. Beneath the heat map is a dendrogram showing hierarchical clustering of the samples. Replicates 1 and 2 in either conditional group are more similar than replicate 3 as is shown. The heat map shows a distinct signature of miRNA

Table 4: Number of differentially expressed miRNA predicted using the multimodel distribution model for each normalization method for each alignment reference generated using the best model approach.

MultiModel

A) Whole genome aligned (p <= 0.05)

	Normalization methods			
	TMM	**TC**	**RPKM**	**TPM**
TMM	59	33	33	6
TC		34	34	7
RPKM			38	10
TPM				33

B) RefSeq Transcripts aligned (p <= 0.05)

	Normalization methods			
	TMM	**TC**	**RPKM**	**TPM**
TMM	63	36	36	13
TC		37	36	14
RPKM			40	17
TPM				39

C) miRBase aligned (p <= 0.05)

	Normalization methods			
	TMM	**TC**	**RPKM**	**TPM**
TMM	254	131	120	120
TC		438	369	368
RPKM			384	381
TPM				381

Table 5: Number of differentially expressed miRNA predicted by the log-normal with shrinkage distribution model for each normalization method for each alignment reference.

Lognormal with shrinkage

A) Whole genome aligned (p <= 0.05)

	Normalization methods			
	TMM	**TC**	**RPKM**	**TPM**
TMM	53	27	27	3
TC		28	27	4
RPKM			29	5
TPM				15

B) RefSeq Transcripts aligned (p <= 0.05)

	Normalization methods			
	TMM	**TC**	**RPKM**	**TPM**
TMM	56	28	28	6
TC		29	28	7
RPKM			33	9
TPM				18

C) miRBase aligned (p <= 0.05)

	Normalization methods			
	TMM	**TC**	**RPKM**	**TPM**
TMM	191	92	72	72
TC		358	296	292
RPKM			307	300
TPM				300

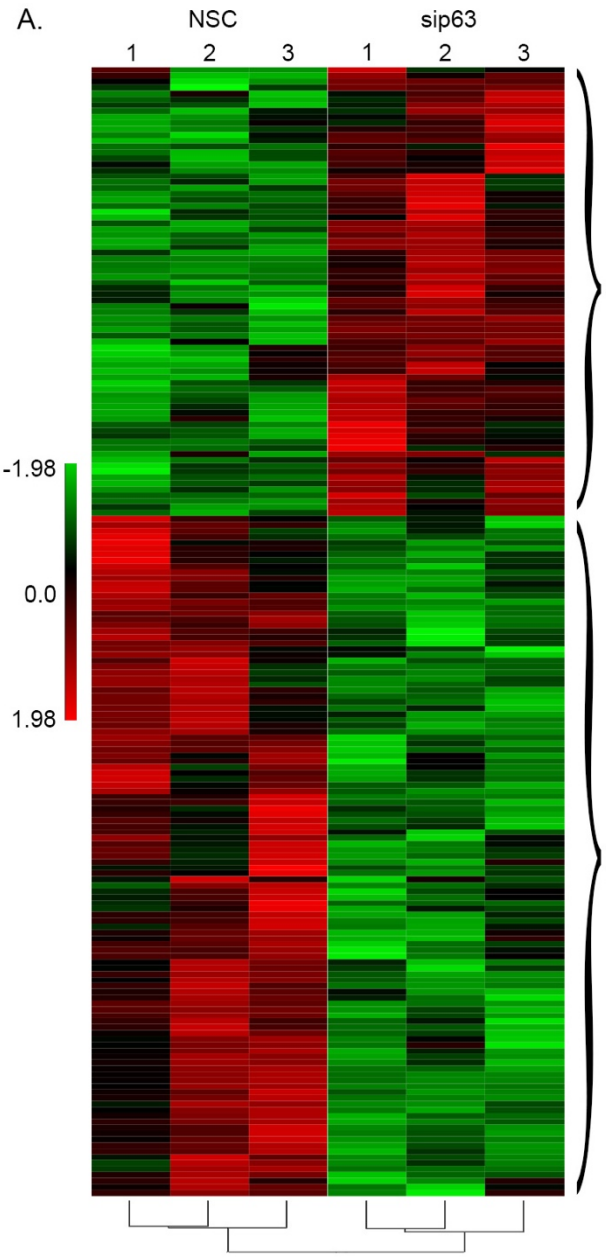

B.

Pathway	Score	p-value
Wnt signaling pathway	9.78	5.65E-05
Morphine addiction	9.31	9.02E-05
Melanogenesis	8.35	0.00024
Notch signaling pathway	7.99	0.00034
Amphetamine addiction	7.80	0.00041
TGF-beta signaling pathway	6.62	0.00133
p53 signaling pathway	6.09	0.00227
Nicotine addiction	6.07	0.00231
Rap1 signaling pathway	5.68	0.00341
Adherens junction	5.64	0.00356
Oocyte meiosis	5.53	0.00396
Signaling pathways regulating pluripotency of stem cells	5.43	0.00438
Other types of O-glycan biosynthesis	5.40	0.00454
Circadian rhythm	5.40	0.00454
Transcriptional misregulation in cancer	5.36	0.00468

C.

Pathway	Score	p-value
Wnt signaling pathway	19.76	2.62E-09
Endocytosis	18.94	5.94E-09
Axon guidance	15.94	1.19E-07
Focal adhesion	15.18	2.55E-07
Hippo signaling pathway	13.27	1.73E-06
Morphine addiction	12.62	3.29E-06
Pathways in cancer	11.89	6.85E-06
Ras signaling pathway	11.50	1.02E-05
Regulation of actin cytoskeleton	10.82	2.00E-05
PI3K-Akt signaling pathway	10.74	2.17E-05
Signaling pathways regulating pluripotency of stem cells	10.47	2.83E-05
Insulin signaling pathway	9.77	5.71E-05
Phosphatidylinositol signaling system	9.36	8.63E-05
TGF-beta signaling pathway	8.97	0.00013
ECM-receptor interaction	8.86	0.00014

Figure 20: Heat map and dendrogram of significant DE miRNAs and pathways they affect. Significant DE miRNAs chosen from miRBase aligned, TMM normalized from LNS approach. A) Heat map and dendrogram generated in Partek flow. B) Pathways affected by miRNAs upregulated in the absence of p63. C) Pathways affected by miRNAs downregulated in the absence of p63.

expression profile as a result of silencing p63. When ΔNp63α is silenced, a subset of miRNAs is upregulated whose target mRNAs encode components in pathways such as Notch signaling and p53. Conversely, when ΔNp63α is silenced, a subset of miRNAs is downregulated who target mRNAs encode for components in pathways related to cancer and PI3K-AKT signaling pathway.

iv. Validation of significantly differentially expressed miRNAs

I obtained the list of 191 differentially expressed miRNAs from miRBase aligned, TMM normalized reads, filtered by a significant p-value of less than or equal to 0.05 (**Table 6**). miRNAs that had high reads (>100) were considered as potential candidates to validate for the purposes of confirming my small RNA-Seq DE results as well as assessing the robustness of the established pipeline. Out of these miRNAs, those that were not previously shown to be regulated by p63 were shortlisted for validation for novel discovery. 15 miRNAs were selected to be validated via qRT-PCR (**Table 7**). miRs-103a-3p, 149-5p, 18a-5p, 19b-1-5p, 590-5p, 598-3p, 7-5p, 708-5p, 744-5p, and 93-5p were all downregulated when ΔNp63α was silenced, thus confirming the DE results detected by small RNA-Seq (**Fig. 22**). By contrast, let-7c-5p, let-7e-5p, and miR-20a-5p did not appear to be regulated as predicted by our small RNA-Seq pipeline's DE analysis.

Table 6: List of miRNAs identified as significantly differently expressed by the small RNA-Seq pipeline. P-value and fold change for each miRNA is listed.

miRNA ID	Avg NSC (reads)			Avg sip63 (reads)			MultiModel p-value	MultiModel Fold-Change
hsa-let-7a-3p	320	+/-	25	160	+/-	11	0.0026	-2.00
hsa-let-7c-5p	2880	+/-	369	1901	+/-	427	0.0346	-1.52
hsa-let-7d-3p	512	+/-	180	304	+/-	50	0.0493	-1.68
hsa-let-7d-5p	10425	+/-	1839	5570	+/-	245	0.0039	-1.87
hsa-let-7e-5p	7740	+/-	1076	5265	+/-	712	0.0479	-1.47
hsa-let-7f-1-3p	513	+/-	97	332	+/-	72	0.0422	-1.55
hsa-miR-100-5p	7757	+/-	638	4728	+/-	1538	0.0190	-1.64
hsa-miR-101-3p	1225	+/-	134	820	+/-	164	0.0384	-1.49
hsa-miR-103a-2-5p	118	+/-	16	67	+/-	27	0.0337	-1.75
hsa-miR-103a-3p	9524	+/-	1779	5177	+/-	239	0.0050	-1.84
hsa-miR-103b	9524	+/-	1779	5177	+/-	239	0.0050	-1.84
hsa-miR-106a-5p	829	+/-	76	510	+/-	48	0.0137	-1.63
hsa-miR-107	1545	+/-	323	823	+/-	91	0.0044	-1.88
hsa-miR-10a-3p	299	+/-	95	706	+/-	298	0.0049	2.36
hsa-miR-10b-3p	8	+/-	3	27	+/-	6	0.0057	3.41
hsa-miR-10b-5p	47	+/-	6	20	+/-	12	0.0189	-2.32
hsa-miR-1180-3p	342	+/-	62	147	+/-	53	0.0017	-2.33
hsa-miR-1199-3p	34	+/-	10	76	+/-	16	0.0096	2.23
hsa-miR-1227-5p	13	+/-	4	3	+/-	2	0.0179	-4.21
hsa-miR-1307-3p	279	+/-	42	176	+/-	20	0.0331	-1.59
hsa-miR-130a-3p	3587	+/-	573	2351	+/-	550	0.0363	-1.53
hsa-miR-138-5p	881	+/-	77	511	+/-	93	0.0085	-1.72
hsa-miR-144-5p	56	+/-	10	30	+/-	6	0.0378	-1.85
hsa-miR-146b-3p	14	+/-	6	34	+/-	10	0.0248	2.35
hsa-miR-149-5p	796	+/-	56	450	+/-	27	0.0051	-1.77
hsa-miR-152-3p	103	+/-	28	38	+/-	21	0.0039	-2.68
hsa-miR-155-3p	59	+/-	28	20	+/-	18	0.0292	-2.90
hsa-miR-17-3p	1346	+/-	130	895	+/-	71	0.0300	-1.50
hsa-miR-181a-2-3p	328	+/-	30	210	+/-	81	0.0429	-1.56
hsa-miR-181b-3p	76	+/-	22	42	+/-	13	0.0479	-1.82
hsa-miR-181b-5p	1639	+/-	333	946	+/-	108	0.0094	-1.73
hsa-miR-182-5p	877	+/-	226	554	+/-	118	0.0393	-1.58
hsa-miR-185-5p	3092	+/-	499	1656	+/-	106	0.0029	-1.87
hsa-miR-188-5p	42	+/-	2	22	+/-	6	0.0374	-1.91
hsa-miR-18a-5p	13957	+/-	642	7916	+/-	1304	0.0066	-1.76
hsa-miR-1908-5p	28	+/-	10	53	+/-	9	0.0415	1.87

hsa-miR-191-5p	4326	+/-	640	2729	+/-	1036	0.0291	-1.59
hsa-miR-194-3p	249	+/-	100	101	+/-	36	0.0048	-2.45
hsa-miR-1973	9	+/-	7	21	+/-	8	0.0487	2.39
hsa-miR-19b-1-5p	208	+/-	26	122	+/-	20	0.0200	-1.71
hsa-miR-205-3p	575	+/-	235	277	+/-	39	0.0089	-2.08
hsa-miR-205-5p	229055	+/-	40315	104386	+/-	18851	0.0042	-2.19
hsa-miR-20a-5p	39907	+/-	3031	25285	+/-	3097	0.0303	-1.58
hsa-miR-210-3p	1505	+/-	287	735	+/-	131	0.0019	-2.05
hsa-miR-211-5p	47	+/-	9	15	+/-	12	0.0078	-3.06
hsa-miR-212-5p	12	+/-	3	43	+/-	11	0.0015	3.68
hsa-miR-23c	11275	+/-	1837	6754	+/-	595	0.0140	-1.67
hsa-miR-24-3p	11664	+/-	3552	6237	+/-	102	0.0112	-1.87
hsa-miR-27a-5p	261	+/-	12	137	+/-	28	0.0062	-1.90
hsa-miR-28-3p	973	+/-	154	641	+/-	113	0.0377	-1.52
hsa-miR-2909	10	+/-	9	24	+/-	1	0.0229	2.48
hsa-miR-299-3p	74	+/-	14	33	+/-	21	0.0120	-2.25
hsa-miR-29b-3p	69244	+/-	3231	41781	+/-	6427	0.0229	-1.66
hsa-miR-29c-3p	3323	+/-	322	2269	+/-	190	0.0387	-1.46
hsa-miR-29c-5p	93	+/-	33	44	+/-	11	0.0206	-2.10
hsa-miR-3130-3p	34	+/-	12	4	+/-	4	0.0005	-8.18
hsa-miR-3135a	11	+/-	5	1	+/-	0	0.0050	-10.81
hsa-miR-3140-3p	51	+/-	13	24	+/-	6	0.0233	-2.12
hsa-miR-3145-5p	22	+/-	2	52	+/-	21	0.0155	2.40
hsa-miR-3160-3p	5	+/-	5	16	+/-	6	0.0258	3.09
hsa-miR-3160-5p	18	+/-	7	5	+/-	5	0.0126	-3.81
hsa-miR-3164	3	+/-	2	12	+/-	5	0.0438	3.45
hsa-miR-3184-5p	72	+/-	28	31	+/-	11	0.0173	-2.33
hsa-miR-3190-3p	1	+/-	0	14	+/-	11	0.0130	12.20
hsa-miR-3192-5p	16	+/-	6	32	+/-	6	0.0467	2.00
hsa-miR-3194-5p	13	+/-	6	29	+/-	9	0.0427	2.19
hsa-miR-3196	10	+/-	5	24	+/-	9	0.0475	2.34
hsa-miR-320a	1624	+/-	121	940	+/-	188	0.0075	-1.73
hsa-miR-320b	948	+/-	100	554	+/-	115	0.0099	-1.71
hsa-miR-320c	191	+/-	34	114	+/-	14	0.0276	-1.67
hsa-miR-324-3p	35	+/-	5	17	+/-	8	0.0446	-2.01
hsa-miR-330-3p	49	+/-	16	23	+/-	11	0.0353	-2.09
hsa-miR-339-5p	2047	+/-	879	1142	+/-	388	0.0348	-1.79
hsa-miR-3529-3p	12104	+/-	4039	5266	+/-	1076	0.0020	-2.30
hsa-miR-363-5p	84	+/-	10	32	+/-	5	0.0017	-2.64
hsa-miR-3649	9	+/-	5	25	+/-	6	0.0173	2.75

hsa-miR-3677-3p	4	+/-	3	14	+/-	7	0.0429	3.20
hsa-miR-3688-3p	18	+/-	27	42	+/-	30	0.0278	2.35
hsa-miR-3689b-5p	2	+/-	2	10	+/-	3	0.0230	4.59
hsa-miR-376c-5p	2	+/-	2	10	+/-	4	0.0323	4.15
hsa-miR-377-3p	19	+/-	5	46	+/-	15	0.0143	2.43
hsa-miR-378a-3p	4317	+/-	997	2303	+/-	226	0.0049	-1.87
hsa-miR-378i	89	+/-	16	40	+/-	12	0.0083	-2.21
hsa-miR-379-3p	44	+/-	14	19	+/-	4	0.0185	-2.32
hsa-miR-3937	51	+/-	16	98	+/-	7	0.0150	1.92
hsa-miR-422a	111	+/-	21	63	+/-	14	0.0339	-1.74
hsa-miR-423-3p	1343	+/-	240	736	+/-	129	0.0058	-1.82
hsa-miR-4298	40	+/-	3	84	+/-	11	0.0078	2.12
hsa-miR-4302	6	+/-	4	19	+/-	7	0.0289	3.22
hsa-miR-4317	26	+/-	8	10	+/-	7	0.0227	-2.66
hsa-miR-4420	9	+/-	1	29	+/-	3	0.0053	3.10
hsa-miR-4438	2	+/-	2	13	+/-	3	0.0083	5.60
hsa-miR-4446-3p	2	+/-	2	11	+/-	6	0.0215	4.79
hsa-miR-4453	10	+/-	5	2	+/-	2	0.0220	-5.40
hsa-miR-4454	3498	+/-	525	2035	+/-	433	0.0097	-1.72
hsa-miR-4477a	7	+/-	2	18	+/-	0	0.0338	2.52
hsa-miR-4492	30	+/-	8	12	+/-	12	0.0377	-2.43
hsa-miR-4494	4	+/-	3	22	+/-	16	0.0130	5.03
hsa-miR-4498	102	+/-	62	228	+/-	105	0.0162	2.24
hsa-miR-449b-5p	14	+/-	6	31	+/-	4	0.0360	2.12
hsa-miR-449c-5p	15	+/-	4	6	+/-	6	0.0457	-2.57
hsa-miR-4511	38	+/-	9	73	+/-	10	0.0195	1.95
hsa-miR-4524a-3p	11	+/-	6	29	+/-	8	0.0254	2.52
hsa-miR-4535	10	+/-	6	2	+/-	2	0.0344	-4.97
hsa-miR-455-3p	964	+/-	328	535	+/-	271	0.0256	-1.80
hsa-miR-4650-3p	87	+/-	31	45	+/-	25	0.0451	-1.95
hsa-miR-4654	17	+/-	9	5	+/-	5	0.0365	-3.24
hsa-miR-4658	5	+/-	4	14	+/-	6	0.0474	2.99
hsa-miR-4676-3p	193	+/-	79	395	+/-	97	0.0062	2.05
hsa-miR-4677-3p	33	+/-	9	15	+/-	2	0.0346	-2.16
hsa-miR-4700-5p	2	+/-	2	8	+/-	2	0.0354	4.04
hsa-miR-4705	15	+/-	8	47	+/-	14	0.0047	3.05
hsa-miR-4722-3p	46	+/-	9	24	+/-	11	0.0425	-1.95
hsa-miR-4727-3p	9	+/-	7	23	+/-	1	0.0338	2.63
hsa-miR-4732-5p	123	+/-	29	59	+/-	9	0.0090	-2.06
hsa-miR-4734	4	+/-	2	13	+/-	2	0.0262	3.51
hsa-miR-4740-5p	23	+/-	8	10	+/-	5	0.0475	-2.36

hsa-miR-4750-5p	99	+/-	20	165	+/-	49	0.0468	1.68
hsa-miR-4758-3p	42	+/-	3	75	+/-	11	0.0343	1.78
hsa-miR-4780	21	+/-	10	8	+/-	3	0.0498	-2.54
hsa-miR-4800-5p	17	+/-	7	4	+/-	3	0.0150	-4.07
hsa-miR-483-5p	102	+/-	24	56	+/-	16	0.0318	-1.82
hsa-miR-497-5p	36	+/-	7	10	+/-	5	0.0033	-3.62
hsa-miR-5002-3p	19	+/-	5	50	+/-	11	0.0075	2.56
hsa-miR-5006-3p	20	+/-	13	4	+/-	0	0.0111	-4.90
hsa-miR-503-5p	503	+/-	133	249	+/-	42	0.0051	-2.02
hsa-miR-505-5p	66	+/-	17	35	+/-	8	0.0346	-1.89
hsa-miR-507	6	+/-	1	17	+/-	3	0.0238	2.92
hsa-miR-5089-5p	17	+/-	8	36	+/-	4	0.0292	2.10
hsa-miR-509-3-5p	3	+/-	2	14	+/-	3	0.0167	4.06
hsa-miR-5196-3p	90	+/-	27	34	+/-	8	0.0030	-2.68
hsa-miR-520f-3p	8	+/-	3	2	+/-	2	0.0474	-3.90
hsa-miR-539-3p	18	+/-	12	41	+/-	12	0.0238	2.30
hsa-miR-548ah-5p	15	+/-	6	46	+/-	16	0.0061	3.07
hsa-miR-548as-5p	13	+/-	9	30	+/-	8	0.0369	2.22
hsa-miR-548ay-5p	1	+/-	0	6	+/-	2	0.0377	6.23
hsa-miR-548o-3p	20	+/-	5	41	+/-	11	0.0399	2.03
hsa-miR-553	15	+/-	2	35	+/-	10	0.0243	2.28
hsa-miR-557	22	+/-	9	8	+/-	1	0.0345	-2.70
hsa-miR-5584-3p	12	+/-	5	3	+/-	2	0.0297	-3.79
hsa-miR-5681a	16	+/-	11	34	+/-	11	0.0397	2.19
hsa-miR-5693	7	+/-	3	29	+/-	1	0.0017	4.30
hsa-miR-5697	93	+/-	22	169	+/-	45	0.0272	1.81
hsa-miR-5705	23	+/-	7	8	+/-	7	0.0240	-2.99
hsa-miR-590-3p	431	+/-	197	187	+/-	78	0.0116	-2.30
hsa-miR-590-5p	1270	+/-	211	650	+/-	41	0.0022	-1.95
hsa-miR-598-3p	189	+/-	65	106	+/-	54	0.0455	-1.79
hsa-miR-6068	13	+/-	6	4	+/-	3	0.0383	-3.36
hsa-miR-6078	21	+/-	17	45	+/-	9	0.0275	2.12
hsa-miR-642a-5p	11	+/-	9	41	+/-	14	0.0093	3.93
hsa-miR-6499-5p	2	+/-	2	12	+/-	2	0.0099	5.56
hsa-miR-6516-3p	18	+/-	5	5	+/-	5	0.0207	-3.31
hsa-miR-657	6	+/-	1	21	+/-	12	0.0176	3.69
hsa-miR-664b-3p	16	+/-	4	6	+/-	3	0.0442	-2.57
hsa-miR-671-5p	360	+/-	128	196	+/-	26	0.0282	-1.83
hsa-miR-6729-5p	9	+/-	6	22	+/-	2	0.0357	2.31
hsa-miR-6730-5p	54	+/-	16	89	+/-	3	0.0491	1.65
hsa-miR-6732-3p	6	+/-	1	18	+/-	3	0.0161	3.13

hsa-miR-6733-5p	539	+/-	103	331	+/-	99	0.0311	-1.63
hsa-miR-6772-5p	6	+/-	6	16	+/-	2	0.0352	2.68
hsa-miR-6775-5p	63	+/-	12	33	+/-	12	0.0290	-1.92
hsa-miR-6776-3p	13	+/-	7	29	+/-	4	0.0320	2.28
hsa-miR-6793-3p	8	+/-	4	25	+/-	12	0.0296	2.92
hsa-miR-6793-5p	23	+/-	15	46	+/-	11	0.0355	2.02
hsa-miR-6797-3p	51	+/-	17	13	+/-	5	0.0011	-3.97
hsa-miR-6811-5p	2	+/-	2	9	+/-	4	0.0377	4.40
hsa-miR-6822-3p	29	+/-	6	64	+/-	31	0.0310	2.21
hsa-miR-6827-5p	16	+/-	10	4	+/-	3	0.0355	-3.71
hsa-miR-6833-3p	17	+/-	9	35	+/-	3	0.0428	1.99
hsa-miR-6850-5p	38	+/-	8	95	+/-	43	0.0081	2.54
hsa-miR-6865-5p	500	+/-	149	285	+/-	54	0.0187	-1.76
hsa-miR-6893-5p	4	+/-	3	21	+/-	1	0.0055	4.68
hsa-miR-7-5p	6650	+/-	2280	3482	+/-	742	0.0134	-1.91
hsa-miR-708-5p	1977	+/-	83	1354	+/-	206	0.0398	-1.46
hsa-miR-7108-3p	176	+/-	37	98	+/-	46	0.0337	-1.80
hsa-miR-7151-5p	6	+/-	3	17	+/-	5	0.0351	2.77
hsa-miR-7154-5p	10	+/-	5	25	+/-	9	0.0276	2.61
hsa-miR-744-5p	506	+/-	64	281	+/-	56	0.0076	-1.80
hsa-miR-769-5p	518	+/-	99	315	+/-	87	0.0284	-1.64
hsa-miR-770-5p	14	+/-	6	33	+/-	14	0.0390	2.39
hsa-miR-7844-5p	5	+/-	0	15	+/-	4	0.0264	3.15
hsa-miR-7974	59	+/-	21	28	+/-	3	0.0314	-2.11
hsa-miR-8086	17	+/-	8	38	+/-	6	0.0255	2.20
hsa-miR-92a-1-5p	69	+/-	28	25	+/-	11	0.0086	-2.71
hsa-miR-92b-3p	615	+/-	157	383	+/-	110	0.0393	-1.61
hsa-miR-93-3p	307	+/-	64	156	+/-	5	0.0054	-1.96
hsa-miR-93-5p	13999	+/-	2668	8068	+/-	1069	0.0118	-1.74
hsa-miR-942-3p	34	+/-	24	12	+/-	4	0.0378	-2.78
hsa-miR-944	114	+/-	24	53	+/-	13	0.0076	-2.14
hsa-miR-95-5p	13	+/-	6	28	+/-	4	0.0434	2.09
hsa-miR-99b-5p	1571	+/-	131	885	+/-	148	0.0049	-1.77

Table 7: miRNAs selected for validation based on p ≤ 0.05 significance and with no known link to p63.

			small RNA-Seq		qRT-PCR	
miRNA symbol	Avg NSC reads	Avg sip63 reads	p-value	Fold-Change	p-value	Fold-Change
hsa-let-7c-5p	2880 +/- 369	1901 +/- 427	0.0346	-1.52	0.5460	0.97
hsa-let-7e-5p	7740 +/- 1076	5265 +/- 712	0.0479	-1.47	0.5882	0.85
hsa-miR-103a-3p	9524 +/- 1779	5177 +/- 239	0.0050	-1.84	0.0087	-2.10
hsa-miR-149-5p	796 +/- 56	450 +/- 27	0.0051	-1.77	0.1659	-1.65
hsa-miR-18a-5p	13957 +/- 642	7916 +/- 1304	0.0066	-1.76	0.0008	-2.52
hsa-miR-19b-1-5p	208 +/- 26	122 +/- 20	0.0200	-1.71	0.0047	-1.61
hsa-miR-20a-5p	39907 +/- 3031	25285 +/- 3097	0.0303	-1.58	0.5320	-1.08
hsa-miR-590-5p	1270 +/- 211	650 +/- 41	0.0022	-1.95	0.5353	-1.19
hsa-miR-598-3p	189 +/- 65	106 +/- 54	0.0455	-1.79	0.1611	-1.35
hsa-miR-7-5p	6650 +/- 2280	3482 +/- 742	0.0134	-1.91	0.0622	-1.20
hsa-miR-708-5p	1977 +/- 83	1354 +/- 206	0.0398	-1.46	0.0884	-1.49
hsa-miR-744-5p	506 +/- 64	281 +/- 56	0.0076	-1.80	0.0050	-2.22
hsa-miR-93-5p	13999 +/- 2668	8068 +/- 1069	0.0118	-1.74	0.0007	-1.78

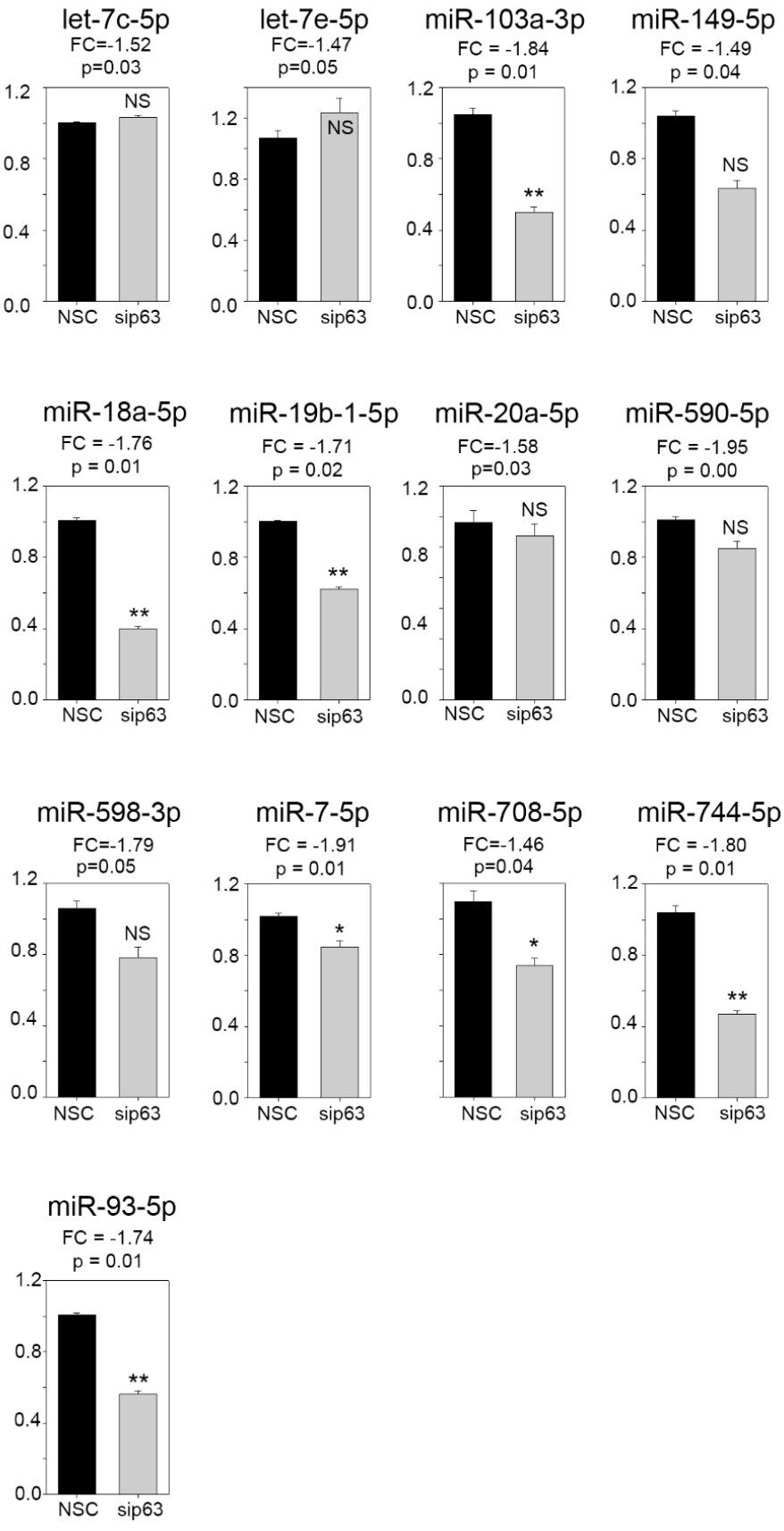
let-7c-5p
FC=-1.52
p=0.03
NS
let-7e-5p
FC=-1.47
p=0.05
NS
miR-103a-3p
FC = -1.84
p = 0.01
**
miR-149-5p
FC = -1.49
p = 0.04
NS
miR-18a-5p
FC = -1.76
p = 0.01
**
miR-19b-1-5p
FC = -1.71
p = 0.02
**
miR-20a-5p
FC=-1.58
p=0.03
NS
miR-590-5p
FC = -1.95
p = 0.00
NS
miR-598-3p
FC=-1.79
p=0.05
NS
miR-7-5p
FC = -1.91
p = 0.01
*
miR-708-5p
FC=-1.46
p=0.04
*
miR-744-5p
FC = -1.80
p = 0.01
**
miR-93-5p
FC = -1.74
p = 0.01
**
0.0
0.4
0.8
1.2
NSC
sip63

Figure 21: qRT-PCR validation of candidate miRNAs. 1 μg of total RNA was reverse transcribed into cDNA and using AODs specific for the candidate miRNAs and quantitative Real-Time PCR was performed. Expression levels were normalized to RNU48. qRT-PCR was done in triplicate for each specific miRNA for each of the 3 biological replicates of NSC and sip63 transfected HaCaT cells. Fold change (FC) and p value information from small RNA-Seq DE analysis listed above. * = $p \leq 0.1$, ** = $p \leq 0.05$, NS = not significant.

IV. DISCUSSION

A. Regulation of ΔNp63α by JNK

In this study, I investigated a novel role for JNK in regulating ΔNp63α in response to genotoxic and carcinogenic stress. A previous study showed that UV damage results in down-regulation of ΔNp63α as a result of phosphorylation of ΔNp63α by p38 MAPK (Liefer, Koster et al. 2000, Papoutsaki, Moretti et al. 2005, Westfall, Joyner et al. 2005). Interestingly, UV exposure led to the activation of not only p38 MAPK signaling pathway, but also the JNK signaling pathway. Specifically, JNK was not ruled out as a potential candidate kinase that phosphorylates ΔNp63α.

I showed that stress-mediated activation of JNK by UV and anisomycin treatment correlated with a mobility shift of ΔNp63α, suggesting phosphorylation of ΔNp63α, which occurred as early as 30 minutes following stress induction. Furthermore, co-expression of ΔNp63α with JNK1 and JNK2 enhanced the ΔNp63α mobility shift. Interestingly, a non-mobility shifted ΔNp63α band or non-phosphorylated form was not observed, suggesting that most, if not all, of the protein was being phosphorylated. An *in vitro* kinase assay with recombinant active JNK1 and JNK2 and recombinant ΔNp63α proteins resulted in ΔNp63α's phosphorylation, suggesting that JNK can bind and phosphorylate ΔNp63α at various residues, which implicates this kinase as a regulator of p63 stability (Chen, Wang et al. 1996). Interestingly, JNK1 had greater phosphorylation effect than JNK2, despite using equal quantities of the kinases in the assay suggesting that JNK1 may have a greater binding affinity for ΔNp63α as compared to JNK2. In the context of non-melanoma skin cancers, this would allow for a cell to undergo apoptosis as opposed to becoming cancerous as JNK1 is known to have tumor suppressor function (Bode and Dong 2007). Specifically, based on our studies, JNK1 would appear to have a more active role in

mediating apoptosis by phosphorylating ΔNp63α, tagging it for ubiquitin-mediated proteasomal degradation.

There is significant homology between p53 family members (Buschmann, Potapova et al. 2001) and as shown in **Figure 6**, JNK targeted residues in TAp73α were highly conserved in ΔNp63α. Mass spectrometry analysis of H1299 cells transfected with ΔNp63α and treated with UV confirmed phosphorylation at several residues which are conserved between ΔNp63α and TAp73 (S53, S66, S369, T297 and T444). While mutation of these residues individually did not prevent the UVC or anisomycin induced mobility shift in ΔNp63α, it is possible that these residues are phosphorylated by active JNK but do not individually cause a mobility shift detectable under the SDS-PAGE conditions used. To address this possibility, a phospho-deficient mutant ΔNp63α containing seven mutated residues was constructed to maximize the likelihood of seeing a reversion of the electrophoretic mobility shift in ΔNp63α. Expressing this mutant in H1299 cells with UV and Anisomycin treatment showed a stabilization of ΔNp63α protein levels, despite a slight mobility shift, suggesting that JNK-mediated phosphorylation is likely due to a combination of sites being phosphorylated and that the phospho-deficient ΔNp63α mutant is no longer targeted for degradation. Alternatively, it cannot be ruled out that mutation of these 7 residues altogether could drastically alter the structure of the protein, and thus, disrupt the interaction between JNK and ΔNp63α. As well, many of these sites are contained in regions that are essential for phosphorylation by p38 (Papoutsaki, Moretti et al. 2005). Differentiating the specific potential residues could be accomplished by creating deletion constructs of recombinant p63 and performing in vitro kinase assays with recombinant active JNK1 or JNK2 to further resolve the specific regions JNK targets and pursuing the serines and threonines within those regions for mutagenesis.

However, my results highlight a previously unrecognized role for JNK signaling as a regulator of ΔNp63α phosphorylation and its subsequent proteasomal degradation following cellular stress.

Future studies will be conducted to closely examine the relationship between active JNK and p63. One potential study will involve using phosphatase controls to show reversion of the electrophoretic mobility shift upon UV or Anisomycin treatment, which would confirm that ΔNp63α is phosphorylated by JNK. Another study will involve studying the association of ΔNp63α and JNK by using immunoprecipitation to test whether JNK binds to ΔNp63α alone or in complex. p73 would be used as positive control as its interaction with JNK is previously known (Jones, Dickman et al. 2007). In addition, the contribution of other MAPK members to the phosphorylation of ΔNp63α will also be explored. This will be done in a preliminary study utilizing a kinase library.

B. ΔNp63α global regulation of miRNA

Next-generation sequencing technology has revolutionized the amount of information that can be gathered about the genetic make-up of organisms, however the platform for data analysis is still a rapidly developing field that requires more studies to accurately confirm that our methods of analysis mirror what is happening biologically. Specifically, there are very few studies that empirically test a next-generation sequencing pipeline workflow parameters for identifying differentially regulated miRNAs for small RNA-Seq data. I aimed to establish an optimized workflow that is suitable for miRNA sequencing data. In this study, NSC and sip63 HaCaT cells were used to optimize next generation sequencing data processing parameters and validate a small RNA-Seq analysis pipeline. The validated pipeline utilizes alignment and quantitation to the miRBase reference, normalization using TMM and a lognormal with shrinkage response

distribution model for the identification of differentially expressed miRNA and has the following benefits: (1) robust annotation and quantitation of miRNA reads compared to alignment using the RefSeq (transcriptome) and Whole Genome reference databases, particularly miRNA with low expression, (2) effective normalization of read distributions leading to the robust clustering of experimental replicates, and (3) concurrence with RT-PCR data. This validated pipeline was used to identify novel ΔNp63α-regulated miRNA which have predicted mRNA targets in cancer signaling pathways. Further characterization of these miRNA and their mRNA targets may provide mechanistic insight into the progression of non-melanoma skin cancer.

Three key steps were taken into consideration for the optimization of the workflow: alignment reference, normalization, and response distribution model for DE analysis. I found that the choice of alignment reference has a major influence on the number of miRNAs that are identified downstream during DE detection. I found that alignments using whole genome and RefSeq Transcripts references yielded a very similar number of differentially expressed miRNAs, whereas alignments using the miRBase reference resulted in a significantly higher number of differentially expressed miRNAs. It is also important to note that alignment to whole genome and RefSeq Transcripts references yielded a large number of aligned reads that did not correspond to a miRNA. Since the default alignment reporting options of the bowtie algorithm were used, with whole genome and RefSeq Transcripts, there was a higher chance of reporting a valid alignment that did not correspond to a miRNA as opposed to reporting one that did correspond with a miRNA, resulting in a higher false negative rate.

Given that miRNA play a regulatory role in gene expression, it is probable that miRNAs are increased or decreased in expression rather than being completely switched on or off. Aligning to miRBase better captures these low basally expressed miRNAs when comparing the differences

in miRNA count distribution. Many more miRNAs were accurately quantified as lowly expressed as opposed to not being quantified at all. This would affect downstream DE detection since even low expressed miRNAs could play a huge role in regulating downstream target mRNA (Tam, Tsao et al. 2015). As well, although the number of total reads that aligned to the miRBase reference was far lower compared to alignment to whole genome or RefSeq Transcripts, a 100% of those aligned reads were quantified as miRNAs. This is due to the usage of default alignment reporting options (reporting 1 valid alignment per read – the first valid alignment Bowtie happens to come across), meaning there was less of a chance of miRBase aligned reads reporting non-specifically aligned reads as would be the case with whole genome or RefSeq Transcripts aligned reads and ultimately being excluded during the quantification process.

Although the normalization step was not initially considered to be crucial in the data analysis process, a similar realization has taken hold with RNA-Seq data much in the same manner of the necessity of normalization with regards to microarray data. DE detection downstream is highly dependent on normalization (Tam, Tsao et al. 2015). We evaluated four different normalization methods (TC, RPKM, TPM, and TMM) on our dataset to identify the most suitable method for normalizing small RNA-Seq data. Upon considering the effects of normalization by relative log expression distribution and clustering of conditional replicates via PCA, I provide compelling evidence that TMM is the most suitable for normalizing small RNA-Seq data. TMM is also supported by previous studies as a robust normalization method (Dillies, Rau et al. 2013, Tam, Tsao et al. 2015).

Differential expression analysis performed using the multimodel or lognormal with shrinkage (LNS) approaches identified a core set of miRNA in our sip63 samples which were differentially expressed relative to NSC samples. The possibility that the multimodel approach

over-fit the data yielding an increased false-positive rate could not be ruled out. ERCC spike-in control RNAs which are routinely used as calibrators for RNA-Seq experiments are not currently configured for use in small RNA-Seq experiments on the Ion Torrent sequencing platform. Thus, assessment of the false-positive rate for the multimodel approach would require extensive qRT-PCR validation, and is beyond the scope of this study. Rather, the LNS approach can be used as a conservative approach for identifying candidate differentially expressed miRNA.

Of the novel p63-regulated miRNA identified and validated in this study, several have known roles in cancer. miR-18a-5p plays an oncogenic role in nasopharyngeal cancer by regulating E-cadherin and K-ras (Luo, Dai et al. 2013), miR-93-5p is elevated in colorectal cancer, and miR-19b-1-5p is downregulated in CD44+ cervical cancer cells which express increased p63 levels, although no link was implied (Xiao, Zhou et al. 2014). Similarly, amplification of the cluster containing miR-20a-5p has been observed in leukemia but only miR-92a, another miRNA in the cluster, is known to regulate p63. Other miRNA identified in this study mediate cancer signaling, such as miR-590-5p which attenuates the TGFβ signaling pathway through down-regulation of SMAD3 and miR-7-5p which targets EGFR (Vasanthan, Govindasamy et al. 2015, Jafarzadeh and Soltani 2016). Nothing has been published regarding the functional roles or regulation for the remaining miRNA identified in this study. It is our hope that these miRNA and additional targets identified by our small RNA-Seq pipeline will be a source of biomarkers and therapeutic targets for p63-related pathologies and provide critical insight into the role played by p63 in cancer.

Within our pipeline workflow, there are, however, challenges to be overcome. In particular, tweaking alignment options to report the best to worst alignments for reads could improve the overall quantification of miRNAs. The current limitations of my analysis were the number of replicates I had for each conditional group. While 3 biological replicates may be enough from the

perspective of a biologist, it is not a big enough sample size to achieve results of high statistical power. Thus, in order to further optimize the pipeline that I have established, future small RNA-Seq experiments involving more replicates for each conditional group would improve the ability for differentially expressed miRNAs to be detected. With regards to novel discovery of p63 biology, miRNAs that were validated could be selected for studies using cell cultures to assess whether its target mRNAs are being regulated and what pathways are being affected.

In conclusion, my investigation of the various alignment reference databases (whole genome, RefSeq and miRBase), normalization methods (TC, RPKM, TPM, and TMM), and response distribution model for DE analysis (Multimodel and LNS) highlights the potential impact of each step on the analysis of small RNA-Seq data. While it is important to experiment with pipeline parameters to accommodate differences in sample library composition and confirm data output by qRT-PCR, I propose that using the Bowtie aligner and the miRBase reference for alignment and quantification as well as the TMM normalization method provide a robust standard pipeline for small RNA-Seq analyses.

REFERENCES

Alisoltani, A., H. Fallahi, B. Shiran, A. Alisoltani and E. Ebrahimie (2015). "RNA-seq SSRs and small RNA-seq SSRs: new approaches in cancer biomarker discovery." Gene **560**(1): 34-43.

Barbieri, C. E., L. J. Tang, K. A. Brown and J. A. Pietenpol (2006). "Loss of p63 leads to increased cell migration and up-regulation of genes involved in invasion and metastasis." Cancer Res **66**(15): 7589-7597.

Bartel, D. P. (2004). "MicroRNAs: genomics, biogenesis, mechanism, and function." Cell **116**(2): 281-297.

Bartel, D. P. (2009). "MicroRNAs: target recognition and regulatory functions." Cell **136**(2): 215-233.

Bircan, S., O. Candir, N. Kapucoglu and S. Baspinar (2006). "The expression of p63 in basal cell carcinomas and association with histological differentiation." J Cutan Pathol **33**(4): 293-298.

Bode, A. M. and Z. Dong (2007). "The functional contrariety of JNK." Mol Carcinog **46**(8): 591-598.

Borchert, G. M., W. Lanier and B. L. Davidson (2006). "RNA polymerase III transcribes human microRNAs." Nat Struct Mol Biol **13**(12): 1097-1101.

Boukamp, P. (2005). "UV-induced skin cancer: similarities--variations." J Dtsch Dermatol Ges **3**(7): 493-503.

Buschmann, T., O. Potapova, A. Bar-Shira, V. N. Ivanov, S. Y. Fuchs, S. Henderson, V. A. Fried, T. Minamoto, D. Alarcon-Vargas, M. R. Pincus, W. A. Gaarde, N. J. Holbrook, Y. Shiloh and Z. Ronai (2001). "Jun NH2-terminal kinase phosphorylation of p53 on Thr-81 is important for p53 stabilization and transcriptional activities in response to stress." Mol Cell Biol **21**(8): 2743-2754.

Carroll, D. K., J. S. Carroll, C. O. Leong, F. Cheng, M. Brown, A. A. Mills, J. S. Brugge and L. W. Ellisen (2006). "p63 regulates an adhesion programme and cell survival in epithelial cells." Nat Cell Biol **8**(6): 551-561.

Chakravarti, D., X. Su, M. S. Cho, N. H. Bui, C. Coarfa, A. Venkatanarayan, A. L. Benham, R. E. Flores Gonzalez, J. Alana, W. Xiao, M. L. Leung, H. Vin, I. L. Chan, A. Aquino, N. Muller, H. Wang, A. J. Cooney, J. Parker-Thornburg, K. Y. Tsai, P. H. Gunaratne and E. R. Flores (2014). "Induced multipotency in adult keratinocytes through down-regulation of DeltaNp63 or DGCR8." Proc Natl Acad Sci U S A **111**(5): E572-581.

Chen, Y. R., X. Wang, D. Templeton, R. J. Davis and T. H. Tan (1996). "The role of c-Jun N-terminal kinase (JNK) in apoptosis induced by ultraviolet C and gamma radiation. Duration of JNK activation may determine cell death and proliferation." J Biol Chem **271**(50): 31929-31936.

Clarke, R., C. Newman, J. Tomson, H. Hin, R. Kurien, J. Cox, M. Lay, J. Sayer, M. Hill, J. Emberson and J. Armitage (2015). "Estimation of the optimum dose of vitamin D for disease prevention in older people: rationale, design and baseline characteristics of the BEST-D trial." Maturitas **80**(4): 426-431.

Conesa, A., P. Madrigal, S. Tarazona, D. Gomez-Cabrero, A. Cervera, A. McPherson, M. W. Szczesniak, D. J. Gaffney, L. L. Elo, X. Zhang and A. Mortazavi (2016). "A survey of best practices for RNA-seq data analysis." Genome Biol **17**: 13.

Courtois, S., C. Caron de Fromentel and P. Hainaut (2004). "p53 protein variants: structural and functional similarities with p63 and p73 isoforms." Oncogene **23**(3): 631-638.

Danilov, A. V., D. Neupane, A. S. Nagaraja, E. V. Feofanova, L. A. Humphries, J. DiRenzo and M. Korc (2011). "DeltaNp63alpha-mediated induction of epidermal growth factor receptor promotes pancreatic cancer cell growth and chemoresistance." PLoS One **6**(10): e26815.

Derijard, B., M. Hibi, I. H. Wu, T. Barrett, B. Su, T. Deng, M. Karin and R. J. Davis (1994). "JNK1: a protein kinase stimulated by UV light and Ha-Ras that binds and phosphorylates the c-Jun activation domain." Cell **76**(6): 1025-1037.

Di Como, C. J., M. J. Urist, I. Babayan, M. Drobnjak, C. V. Hedvat, J. Teruya-Feldstein, K. Pohar, A. Hoos and C. Cordon-Cardo (2002). "p63 expression profiles in human normal and tumor tissues." Clin Cancer Res **8**(2): 494-501.

Di Costanzo, A., L. Festa, O. Duverger, M. Vivo, L. Guerrini, G. La Mantia, M. I. Morasso and V. Calabro (2009). "Homeodomain protein Dlx3 induces phosphorylation-dependent p63 degradation." Cell Cycle **8**(8): 1185-1195.

Dillies, M. A., A. Rau, J. Aubert, C. Hennequet-Antier, M. Jeanmougin, N. Servant, C. Keime, G. Marot, D. Castel, J. Estelle, G. Guernec, B. Jagla, L. Jouneau, D. Laloe, C. Le Gall, B. Schaeffer, S. Le Crom, M. Guedj, F. Jaffrezic and C. French StatOmique (2013). "A comprehensive evaluation of normalization methods for Illumina high-throughput RNA sequencing data analysis." Brief Bioinform **14**(6): 671-683.

Do, C. B. and S. Batzoglou (2008). "What is the expectation maximization algorithm?" Nat Biotechnol **26**(8): 897-899.

Fuchs, S. Y., V. Adler, M. R. Pincus and Z. Ronai (1998). "MEKK1/JNK signaling stabilizes and activates p53." Proc Natl Acad Sci U S A **95**(18): 10541-10546.

Helwak, A., G. Kudla, T. Dudnakova and D. Tollervey (2013). "Mapping the human miRNA interactome by CLASH reveals frequent noncanonical binding." Cell **153**(3): 654-665.

Hibi, M., A. Lin, T. Smeal, A. Minden and M. Karin (1993). "Identification of an oncoprotein- and UV-responsive protein kinase that binds and potentiates the c-Jun activation domain." Genes Dev **7**(11): 2135-2148.

Hill, N. T., J. Zhang, M. K. Leonard, M. Lee, H. N. Shamma and M. Kadakia (2015). "1alpha, 25-Dihydroxyvitamin D(3) and the vitamin D receptor regulates DeltaNp63alpha levels and keratinocyte proliferation." Cell Death Dis **6**: e1781.

Hochedlinger, K., E. F. Wagner and K. Sabapathy (2002). "Differential effects of JNK1 and JNK2 on signal specific induction of apoptosis." Oncogene **21**(15): 2441-2445.

Hu, M. C., W. R. Qiu and Y. P. Wang (1997). "JNK1, JNK2 and JNK3 are p53 N-terminal serine 34 kinases." Oncogene **15**(19): 2277-2287.

Irani, S. (2016). "miRNAs Signature in Head and Neck Squamous Cell Carcinoma Metastasis: A Literature Review." J Dent (Shiraz) **17**(2): 71-83.

Jafarzadeh, M. and B. M. Soltani (2016). "Hsa-miR-590-5p Interaction with SMAD3 Transcript Supports Its Regulatory Effect on The TGFbeta Signaling Pathway." Cell J **18**(1): 7-12.

Jansson, M. D. and A. H. Lund (2012). "MicroRNA and cancer." Mol Oncol **6**(6): 590-610.

Jones, E. V., M. J. Dickman and A. J. Whitmarsh (2007). "Regulation of p73-mediated apoptosis by c-Jun N-terminal kinase." Biochem J **405**(3): 617-623.

Katoh, I., K. I. Aisaki, S. I. Kurata, S. Ikawa and Y. Ikawa (2000). "p51A (TAp63gamma), a p53 homolog, accumulates in response to DNA damage for cell regulation." Oncogene **19**(27): 3126-3130.

Kommagani, R., T. M. Caserta and M. P. Kadakia (2006). "Identification of vitamin D receptor as a target of p63." Oncogene **25**(26): 3745-3751.

Kommagani, R., M. K. Leonard, S. Lewis, R. A. Romano, S. Sinha and M. P. Kadakia (2009). "Regulation of VDR by deltaNp63alpha is associated with inhibition of cell invasion." J Cell Sci **122**(Pt 16): 2828-2835.

Koster, M. I., S. Kim, A. A. Mills, F. J. DeMayo and D. R. Roop (2004). "p63 is the molecular switch for initiation of an epithelial stratification program." Genes Dev **18**(2): 126-131.

Koster, M. I. and D. R. Roop (2004). "The role of p63 in development and differentiation of the epidermis." J Dermatol Sci **34**(1): 3-9.

Koster, M. I. and D. R. Roop (2004). "Transgenic mouse models provide new insights into the role of p63 in epidermal development." Cell Cycle **3**(4): 411-413.

Kou, Y., L. Qiao and Q. Wang (2015). "Identification of core miRNA based on small RNA-seq and RNA-seq for colorectal cancer by bioinformatics." Tumour Biol **36**(4): 2249-2255.

Langmead, B., C. Trapnell, M. Pop and S. L. Salzberg (2009). "Ultrafast and memory-efficient alignment of short DNA sequences to the human genome." Genome Biol **10**(3): R25.

Langmead, C. J. and S. K. Jha (2009). "Symbolic approaches for finding control strategies in Boolean Networks." J Bioinform Comput Biol **7**(2): 323-338.

Law, C. W., Y. Chen, W. Shi and G. K. Smyth (2014). "voom: Precision weights unlock linear model analysis tools for RNA-seq read counts." Genome Biol **15**(2): R29.

Lazzari, C., A. Prodosmo, F. Siepi, C. Rinaldo, F. Galli, M. Gentileschi, A. Bartolazzi, A. Costanzo, A. Sacchi, L. Guerrini and S. Soddu (2011). "HIPK2 phosphorylates DeltaNp63alpha and promotes its degradation in response to DNA damage." Oncogene **30**(48): 4802-4813.

Lee, Y., M. Kim, J. Han, K. H. Yeom, S. Lee, S. H. Baek and V. N. Kim (2004). "MicroRNA genes are transcribed by RNA polymerase II." EMBO J **23**(20): 4051-4060.

Leonard, M. K., R. Kommagani, V. Payal, L. D. Mayo, H. N. Shamma and M. P. Kadakia (2011). "DeltaNp63alpha regulates keratinocyte proliferation by controlling PTEN expression and localization." Cell Death Differ **18**(12): 1924-1933.

Lewis, B. P., C. B. Burge and D. P. Bartel (2005). "Conserved seed pairing, often flanked by adenosines, indicates that thousands of human genes are microRNA targets." Cell **120**(1): 15-20.

Li, B. and C. N. Dewey (2011). "RSEM: accurate transcript quantification from RNA-Seq data with or without a reference genome." BMC Bioinformatics **12**: 323.

Li, X., Y. Shen, H. Ichikawa, T. Antes and G. S. Goldberg (2009). "Regulation of miRNA expression by Src and contact normalization: effects on nonanchored cell growth and migration." Oncogene **28**(48): 4272-4283.

Liefer, K. M., M. I. Koster, X. J. Wang, A. Yang, F. McKeon and D. R. Roop (2000). "Down-regulation of p63 is required for epidermal UV-B-induced apoptosis." Cancer Res **60**(15): 4016-4020.

Lin, C., X. Li, Y. Zhang, Y. Guo, J. Zhou, K. Gao, J. Dai, G. Hu, L. Lv, J. Du and Y. Zhang (2015). "The microRNA feedback regulation of p63 in cancer progression." Oncotarget **6**(11): 8434-8453.

Lin, L. J., Y. Lin, Y. Jin and C. Q. Zheng (2014). "Investigation of key microRNAs associated with hepatocellular carcinoma using small RNA-seq data." Mol Biol Rep **41**(7): 4341-4349.

Lo Muzio, L., A. Santarelli, R. Caltabiano, C. Rubini, T. Pieramici, L. Trevisiol, F. Carinci, R. Leonardi, A. De Lillo, S. Lanzafame, P. Bufo and A. Piattelli (2005). "p63 overexpression associates with poor prognosis in head and neck squamous cell carcinoma." Hum Pathol **36**(2): 187-194.

Lu, J., G. Getz, E. A. Miska, E. Alvarez-Saavedra, J. Lamb, D. Peck, A. Sweet-Cordero, B. L. Ebert, R. H. Mak, A. A. Ferrando, J. R. Downing, T. Jacks, H. R. Horvitz and T. R. Golub (2005). "MicroRNA expression profiles classify human cancers." Nature **435**(7043): 834-838.

Luo, Z., Y. Dai, L. Zhang, C. Jiang, Z. Li, J. Yang, J. B. McCarthy, X. She, W. Zhang, J. Ma, W. Xiong, M. Wu, J. Lu, X. Li, X. Li, J. Xiang and G. Li (2013). "miR-18a promotes malignant progression by impairing microRNA biogenesis in nasopharyngeal carcinoma." Carcinogenesis **34**(2): 415-425.

Marinari, B., C. Ballaro, M. I. Koster, M. L. Giustizieri, F. Moretti, F. Crosti, M. Papoutsaki, M. Karin, S. Alema, S. Chimenti, D. R. Roop and A. Costanzo (2009). "IKKalpha is a p63 transcriptional target involved in the pathogenesis of ectodermal dysplasias." J Invest Dermatol **129**(1): 60-69.

Masse, I., L. Barbollat-Boutrand, M. Molina, O. Berthier-Vergnes, N. Joly-Tonetti, M. T. Martin, C. Caron de Fromentel, J. Kanitakis and J. Lamartine (2012). "Functional interplay between p63 and p53 controls RUNX1 function in the transition from proliferation to differentiation in human keratinocytes." Cell Death Dis **3**: e318.

Medina-Franco, H., L. O. Vasconez, R. J. Fix, M. J. Heslin, S. W. Beenken, K. I. Bland and M. M. Urist (2002). "Factors associated with local recurrence after skin-sparing mastectomy and immediate breast reconstruction for invasive breast cancer." Ann Surg **235**(6): 814-819.

Mills, A. A., B. Zheng, X. J. Wang, H. Vogel, D. R. Roop and A. Bradley (1999). "p63 is a p53 homologue required for limb and epidermal morphogenesis." Nature **398**(6729): 708-713.

Mortazavi, A., B. A. Williams, K. McCue, L. Schaeffer and B. Wold (2008). "Mapping and quantifying mammalian transcriptomes by RNA-Seq." Nat Methods **5**(7): 621-628.

Okada, Y., M. Osada, S. Kurata, S. Sato, K. Aisaki, Y. Kageyama, K. Kihara, Y. Ikawa and I. Katoh (2002). "p53 gene family p51(p63)-encoded, secondary transactivator p51B(TAp63alpha) occurs without forming an immunoprecipitable complex with MDM2, but responds to genotoxic stress by accumulation." Exp Cell Res **276**(2): 194-200.

Ortt, K., E. Raveh, U. Gat and S. Sinha (2008). "A chromatin immunoprecipitation screen in mouse keratinocytes reveals Runx1 as a direct transcriptional target of DeltaNp63." J Cell Biochem **104**(4): 1204-1219.

Osada, M., H. L. Park, Y. Nagakawa, K. Yamashita, A. Fomenkov, M. S. Kim, G. Wu, S. Nomoto, B. Trink and D. Sidransky (2005). "Differential recognition of response elements determines target gene specificity for p53 and p63." Mol Cell Biol **25**(14): 6077-6089.

Oshlack, A., M. D. Robinson and M. D. Young (2010). "From RNA-seq reads to differential expression results." Genome Biol **11**(12): 220.

Papoutsaki, M., F. Moretti, M. Lanza, B. Marinari, V. Sartorelli, L. Guerrini, S. Chimenti, M. Levrero and A. Costanzo (2005). "A p38-dependent pathway regulates DeltaNp63 DNA binding to p53-dependent promoters in UV-induced apoptosis of keratinocytes." Oncogene **24**(46): 6970-6975.

Park, G. B., Y. S. Kim, H. K. Lee, J. W. Yang, D. Kim and D. Y. Hur (2016). "ASK1/JNK-mediated TAp63 activation controls the cell survival signal of baicalein-treated EBV-transformed B cells." Mol Cell Biochem **412**(1-2): 247-258.

Pellegrini, G., E. Dellambra, O. Golisano, E. Martinelli, I. Fantozzi, S. Bondanza, D. Ponzin, F. McKeon and M. De Luca (2001). "p63 identifies keratinocyte stem cells." Proc Natl Acad Sci U S A **98**(6): 3156-3161.

Raingeaud, J., S. Gupta, J. S. Rogers, M. Dickens, J. Han, R. J. Ulevitch and R. J. Davis (1995). "Pro-inflammatory cytokines and environmental stress cause p38 mitogen-activated protein kinase activation by dual phosphorylation on tyrosine and threonine." J Biol Chem **270**(13): 7420-7426.

Ramskold, D., E. Kavak and R. Sandberg (2012). "How to analyze gene expression using RNA-sequencing data." Methods Mol Biol **802**: 259-274.

Ratovitski, E. A. (2013). "Tumor Protein p63/microRNA Network in Epithelial Cancer Cells." Curr Genomics **14**(7): 441-452.

Reis-Filho, J. S., B. Torio, A. Albergaria and F. C. Schmitt (2002). "p63 expression in normal skin and usual cutaneous carcinomas." J Cutan Pathol **29**(9): 517-523.

Robinson, M. D. and A. Oshlack (2010). "A scaling normalization method for differential expression analysis of RNA-seq data." Genome Biol **11**(3): R25.

Rodriguez Calleja, L., C. Jacques, F. Lamoureux, M. Baud'huin, M. Tellez Gabriel, T. Quillard, D. Sahay, P. Perrot, J. Amiaud, C. Charrier, R. Brion, F. Lecanda, F. Verrecchia, D. Heymann, L. W. Ellisen and B. Ory (2016). "DeltaNp63alpha Silences a miRNA Program to Aberrantly Initiate a Wound-Healing Program That Promotes TGFbeta-Induced Metastasis." Cancer Res **76**(11): 3236-3251.

Rogers, H. W., M. A. Weinstock, S. R. Feldman and B. M. Coldiron (2015). "Incidence Estimate of Nonmelanoma Skin Cancer (Keratinocyte Carcinomas) in the U.S. Population, 2012." JAMA Dermatol **151**(10): 1081-1086.

Sabapathy, K., K. Hochedlinger, S. Y. Nam, A. Bauer, M. Karin and E. F. Wagner (2004). "Distinct roles for JNK1 and JNK2 in regulating JNK activity and c-Jun-dependent cell proliferation." Mol Cell **15**(5): 713-725.

Safai, B. and R. A. Good (1977). "Basal cell carcinoma with metastasis. Review of literature." Arch Pathol Lab Med **101**(6): 327-331.

Senoo, M., Y. Matsumura and S. Habu (2002). "TAp63gamma (p51A) and dNp63alpha (p73L), two major isoforms of the p63 gene, exert opposite effects on the vascular endothelial growth factor (VEGF) gene expression." Oncogene **21**(16): 2455-2465.

Tam, S., M. S. Tsao and J. D. McPherson (2015). "Optimization of miRNA-seq data preprocessing." Brief Bioinform **16**(6): 950-963.

Urist, M. J., C. J. Di Como, M. L. Lu, E. Charytonowicz, D. Verbel, C. P. Crum, T. A. Ince, F. D. McKeon and C. Cordon-Cardo (2002). "Loss of p63 expression is associated with tumor progression in bladder cancer." Am J Pathol **161**(4): 1199-1206.

Vasanthan, P., V. Govindasamy, N. Gnanasegaran, W. Kunasekaran, S. Musa and N. H. Abu Kasim (2015). "Differential expression of basal microRNAs' patterns in human dental pulp stem cells." J Cell Mol Med **19**(3): 566-580.

Westfall, M. D., A. S. Joyner, C. E. Barbieri, M. Livingstone and J. A. Pietenpol (2005). "Ultraviolet radiation induces phosphorylation and ubiquitin-mediated degradation of DeltaNp63alpha." Cell Cycle **4**(5): 710-716.

Wojcicka, A., M. Kolanowska and K. Jazdzewski (2016). "MECHANISMS IN ENDOCRINOLOGY: MicroRNA in diagnostics and therapy of thyroid cancer." Eur J Endocrinol **174**(3): R89-98.

Wu, G. S. (2004). "The functional interactions between the p53 and MAPK signaling pathways." Cancer Biol Ther **3**(2): 156-161.

Wu, H., C. Wang and Z. Wu (2013). "A new shrinkage estimator for dispersion improves differential expression detection in RNA-seq data." Biostatistics **14**(2): 232-243.

Xiao, S., Y. Zhou, J. Jiang, L. Yuan and M. Xue (2014). "CD44 affects the expression level of FOSlike antigen 1 in cervical cancer tissues." Mol Med Rep **9**(5): 1667-1674.

Yang, A., M. Kaghad, D. Caput and F. McKeon (2002). "On the shoulders of giants: p63, p73 and the rise of p53." Trends Genet **18**(2): 90-95.

Yang, A., M. Kaghad, Y. Wang, E. Gillett, M. D. Fleming, V. Dotsch, N. C. Andrews, D. Caput and F. McKeon (1998). "p63, a p53 homolog at 3q27-29, encodes multiple products with transactivating, death-inducing, and dominant-negative activities." Mol Cell **2**(3): 305-316.

Yang, A., R. Schweitzer, D. Sun, M. Kaghad, N. Walker, R. T. Bronson, C. Tabin, A. Sharpe, D. Caput, C. Crum and F. McKeon (1999). "p63 is essential for regenerative proliferation in limb, craniofacial and epithelial development." Nature **398**(6729): 714-718.

Yuan, M., P. Luong, C. Hudson, K. Gudmundsdottir and S. Basu (2010). "c-Abl phosphorylation of DeltaNp63alpha is critical for cell viability." Cell Death Dis **1**: e16.

Zeng, Y. and B. R. Cullen (2004). "Structural requirements for pre-microRNA binding and nuclear export by Exportin 5." Nucleic Acids Res **32**(16): 4776-4785.

Zhang, J. and G. T. Bowden (2012). "Activation of p38 MAP kinase and JNK pathways by UVA irradiation." Photochem Photobiol Sci **11**(1): 54-61.

Zhang, J. Y. and M. A. Selim (2012). "The role of the c-Jun N-terminal Kinase signaling pathway in skin cancer." Am J Cancer Res **2**(6): 691-698.